iScience

CellPress
OPEN ACCESS

Article

Conformational Dynamics of Nonenveloped Circovirus Capsid to the Host Cell Receptor

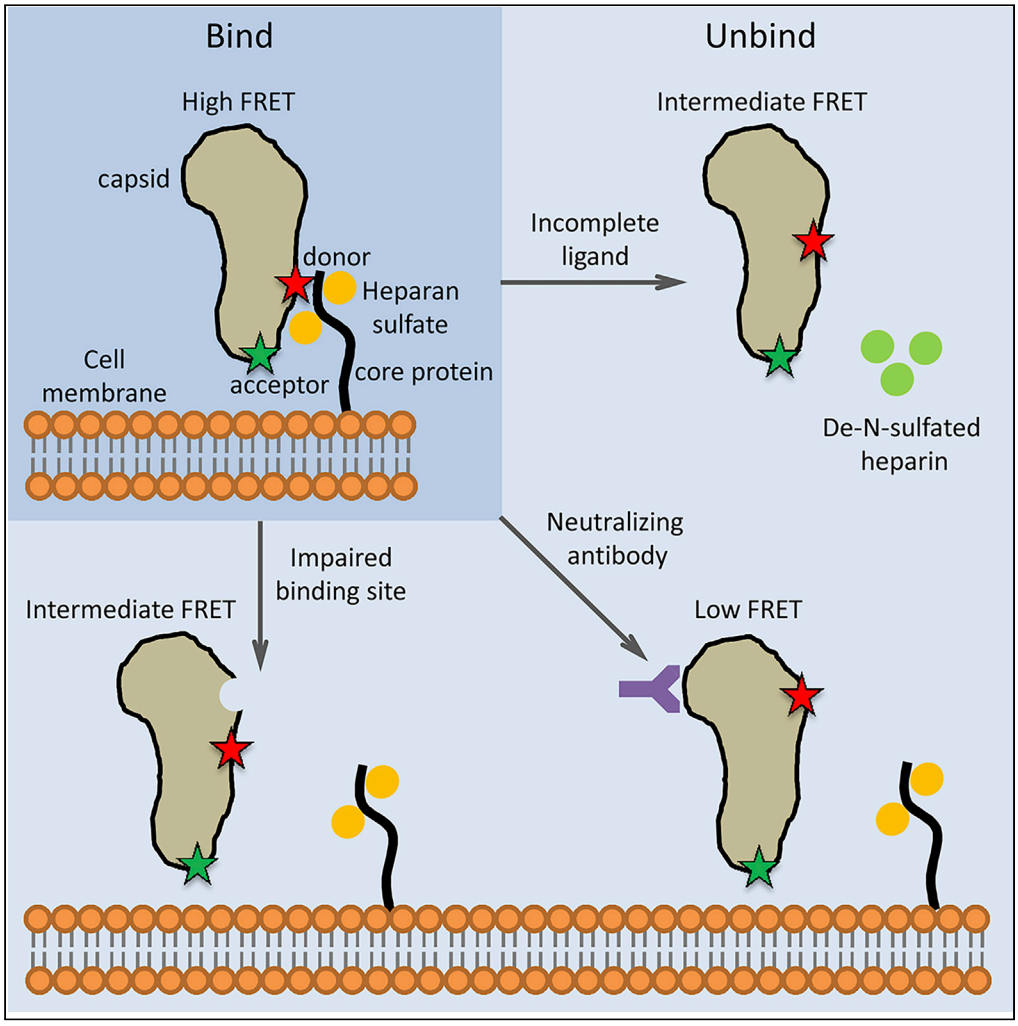

Jiarong Li, Jinyan Gu, Cui Lin, ..., Fengcai Wen, Bo Sun, Jiyong Zhou

gujinyan@zju.edu.cn (J.G.)
jyzhou@zju.edu.cn (J.Z.)

HIGHLIGHTS

Circovirus capsid samples have spontaneous and reversible conformations

Receptor binding regulates capsid dynamics

Capsid encountering with receptor induces the exposure of the receptor-binding site

Capsid interaction with the neutralizing antibody can return to the original conformation

Li et al., iScience *23*, 101547
October 23, 2020
https://doi.org/10.1016/j.isci.2020.101547

iScience

CellPress
OPEN ACCESS

Article

Conformational Dynamics of Nonenveloped Circovirus Capsid to the Host Cell Receptor

Jiarong Li,[1,5] Jinyan Gu,[1,5,6,*] Cui Lin,[1] Jianwei Zhou,[1] Shengnan Wang,[1] Jin Lei,[2] Fengcai Wen,[4] Bo Sun,[4] and Jiyong Zhou[1,3,*]

SUMMARY

Circovirus, comprising one capsid protein, is the smallest nonenveloped virus and induces lymphopenia. Circovirus can be used to explore the cell adhesion mechanism of nonenveloped viruses. We developed a single-molecule fluorescence resonance energy transfer (smFRET) assay to directly visualize the capsid's conformational feature. The capsid underwent reversible dynamic transformation between three conformations. The cell surface receptor heparan sulfate (HS) altered the dynamic equilibrium of the capsid to the high-FRET state, revealing the HS-binding region. Neutralizing antibodies restricted capsid transition to a low-FRET state, masking the HS-binding domain. The lack of positively charged amino acids in the HS-binding site reduced cell surface affinity and attenuated virus infectivity via conformational changes. These intrinsic characteristics of the capsid suggested that conformational dynamics is critical for the structural changes occurring upon cell surface receptor binding, supporting a dynamics-based mechanism of receptor binding.

INTRODUCTION

Virus attachment to the host cell surface is the initial step in establishing effective infection. The host cell membranes are abundantly decorated with proteoglycans, which comprise a core protein and several types of covalently attached glycosaminoglycan chains (GAGs) that are capable of binding protein ligands (Kjellen and Lindahl, 1991; Rostand and Esko, 1997). GAGs include heparan sulfate (HS), chondroitin sulfate (CS), and keratan sulfate, which are characterized by disaccharide repeating units that form the blocks of the polysaccharides (Li and Spillmann, 2012; Prydz and Dalen, 2000; Sarrazin et al., 2011). Epimerization and terminal sulfation are the most common modification patterns during the processing of GAG chains and are also vital for the binding properties of the ligands (Bernfield et al., 1999; Zautner et al., 2006). Among these GAGs, HS is utilized by numerous viruses for attachment to cell surfaces, such as the hepatitis C virus (Xu et al., 2015), human enterovirus 71 (Tan et al., 2013), rabies virus (Sasaki et al., 2018), human papillomavirus type 11 (Joyce et al., 1999), porcine epidemic diarrhea virus (Huan et al., 2015), and porcine circovirus type 2 (PCV2) (Misinzo et al., 2006). The canonical HS-binding motif has been identified as "XBBXBX" or "XBBBXXBX" ("B" represents a basic amino acid and "X" represents a neutral/hydrophobic amino acid) through molecular modeling based on authenticated HS-binding protein receptors (Cardin and Weintraub, 1989). However, the regulation of virus-ligand conformational features and the mechanism of binding to HS are unknown.

Since 1996, single-molecule fluorescence resonance energy transfer (smFRET) has been used to analyze replication, transcription, translation, RNA folding, non-canonical DNA dynamics, and protein conformational changes (Ha, 2001; Ha et al., 1996; Michalet et al., 2006). The envelope glycoprotein of enveloped viruses is a membrane fusion machine that promotes viral entry into host cells. To date, the conformation dynamics of the envelope glycoproteins of HIV-1 and flu virus have been analyzed. The glycoprotein gp120 of the HIV-1 envelope was shown to have three distinct pre-fusion conformations, whose relative occupancies were remodeled by receptor CD4 and antibody binding (Munro et al., 2014). In addition, the hemagglutinin of the flu virus envelope was revealed to undergo reversible exchange between the pre-fusion and two intermediate conformations (Das et al., 2018). However, for the numerous nonenveloped viruses, the direct visualization and conformational dynamic assessment of the capsid remain unreported.

[1]MOA Key Laboratory of Animal Virology, Center for Veterinary Sciences, Zhejiang University, Hangzhou, Zhejiang 310058, China

[2]Institute of Immunology and College of Veterinary Medicine, Nanjing Agricultural University, Nanjing 210095, China

[3]Collaborative Innovation Center and State Key Laboratory for Diagnosis and Treatment of Infectious Diseases, The First Affiliated Hospital, Zhejiang University, Hangzhou, Zhejiang 310058, China

[4]School of Life Science and Technology, ShanghaiTech University, Shanghai, 201210, China

[5]These authors contributed equally

[6]Lead Contact

*Correspondence: gujinyan@zju.edu.cn (J.G.), jyzhou@zju.edu.cn (J.Z.)

https://doi.org/10.1016/j.isci.2020.101547

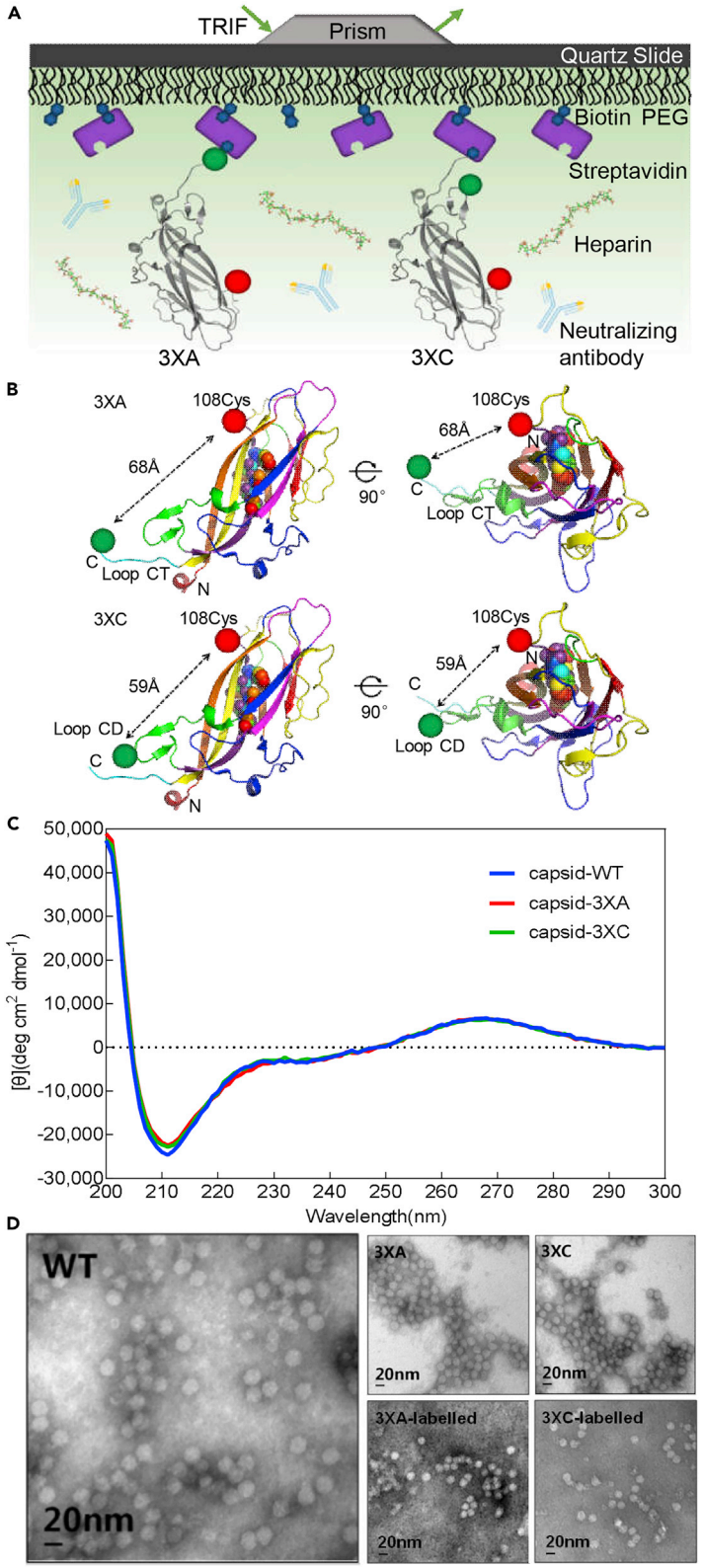
A
TRIF
Prism
Quartz Slide
Biotin PEG
Streptavidin
Heparin
Neutralizing antibody
3XA
3XC
B
3XA
108Cys
68Å
C
Loop CT
N
90°
3XC
59Å
Loop CD
C
N
C
50,000
40,000
30,000
20,000
10,000
0
-10,000
-20,000
-30,000
200
210
220
230
240
250
260
270
280
290
300
Wavelength(nm)
[θ](deg cm2 dmol-1)
capsid-WT
capsid-3XA
capsid-3XC
D
WT
20nm
3XA
3XC
3XA-labelled
3XC-labelled

Figure 1. Single-Molecule FRET Method for Direct Capsid Visualization

(A) Schematic of the smFRET imaging assay. Capsid 3XA or 3XC protein monomers containing a single pair of dually labeled fluorophores were immobilized on quartz microscope slides and imaged using TIRF microscopy at room temperature.

(B) Structural molecular models of Cy5/DY-547-labeled capsid. Fluorophores Cy5 (red ball) and DY-547 (green ball) were placed at the ^{108}Cysteine residue and at the C-terminal loop (3XA) or at the CD loop (3XC), respectively. The predicted distances between labeled sites in capsid meet the technical limitation of smFRET experiments. The putative HS-binding site within the capsid is represented as a sphere. All the structures were adapted from PDB: 3R0R.

(C) Circular dichroism assay of the secondary structure of soluble WT, 3XA, and 3XC capsids. The spectrum curve of the samples was acquired from the ellipticity data measured at a wavelength of 200–300 nm.

(D) Transmission electron microscopic imaging of PCV2 virus-like particles. Capsid-WT, capsid-3XA, capsid-3XC, labeled capsid-3XA, and capsid-3XC assembled into a hexagonal particle with a diameter of 17 nm.

See also Figure S1

Circovirus is the smallest nonenveloped icosahedral virus, with a circular, single-stranded genomic DNA, which infects a variety of species ranging from animals to plants with different pathogenicities (Dennis et al., 2018). PCV2, with a unique structural capsid protein, is a representative circovirus that causes significant morbidity and mortality in swine (Allan and Ellis, 2000; Finsterbusch and Mankertz, 2009; Nawagitgul et al., 2000). The crystal structure of the PCV2 virus-like particle (VLP) revealed that the capsid protein comprises two β-sheets, each containing four antiparallel β-strands, which were labeled as B to I (Khayat et al., 2011). The residues between the β-strands form eight loops, among which the CD and C-terminal loops are exposed on the VLP exterior and can accommodate the insertion of short foreign peptides (Liu et al., 2016; Wang et al., 2016, 2018). The capsid protein was also reported to have the neutralizing and non-neutralizing epitope sites and the putative canonical HS-binding motif ^{98}IRKVKV^{103} (Mahe et al., 2000; Misinzo et al., 2006; Shang et al., 2009). Recently, Dhindwai et al. also proposed the existence of multiple weak binding sites that interact with HS of the PCV2 VLP surface. However, as the simplest nonenveloped virus, in which the capsid is only composed of one protein, what are the conformational features of the circovirus capsid during binding to the cell surface receptor? Does the binding motif move toward the exterior face of the virus particle to achieve the interaction with the GAG molecules? What is the key factor of the motif and the GAGs that facilitate the interaction by adjusting of the capsid's conformational behavior? In the present study we aimed to answer some of these using the PCV2 capsid and HS as a model to explore the conformational dynamics of nonenveloped virus to cell invasions.

In the present study, we developed an smFRET imaging assay to detect the conformational dynamics of the virus capsid protein. Our results revealed that the capsid worked in a dynamic manner, undergoing spontaneous and reversible transitions between three distinct conformations. The binding of the GAGs and that of neutralizing antibodies shifted the dynamic equilibrium associated with the virus binding to the host cells. Both the negatively and positively charged distribution of the receptor and the binding motif peptides played a critical role in the capsid's conformational dynamics and ultimately influenced the affinity to the cell surface receptor. The allostery of the capsid that occurs during direct interactions with the GAG molecules might provide a strategy by which the circovirus strengthens its attachment to the host cells, ultimately resulting in infection.

RESULTS

Site-Specific Attachment of Fluorophores to the Capsid Protein

To develop an smFRET imaging assay to visualize the conformational dynamics of the PCV2 capsid (Figure 1A), we attached the Cy5 fluorophore (acceptor fluorophore) at position ^{108}Cysteine in the DE loop of the capsid (Figure S1A) (Roy et al., 2008). To install the donor fluorophore, we inserted the A1 Tag peptide (GDSLDMLEWSLM) at position ^{80}Leucine of the CD loop or at position ^{233}Proline of the C-terminal loop, which are relatively non-conserved regions of capsid. Thus, the DY-547 fluorophore was labeled using holo-acyl carrier protein synthetase, which catalyzed serine hydroxylation of the A1 peptide and the 4′-phosphopantetheine moiety of CoA to form a phosphodiester bond (Zhou et al., 2007). The Avi peptides were attached at the C terminus of the capsid to accomplish biotinylation processing via the BirA catalyzation (Figure S1A) (Fairhead and Howarth, 2015). According to previously reported structure of the capsid, these two designed models, termed capsid 3XA (3XA) and capsid 3XC (3XC), were used to demonstrate that the predicted distances between the donor and acceptor fluorophores were about 68 Å (3XA) and 59 Å (3XC) (Figure 1B), which satisfied the demand of the smFRET experiment (Roy et al., 2008). Western

blotting and typhoon assays confirmed that Cy5 was co-localized with DY-547, demonstrating that 3XA and 3XC were specifically labeled with fluorophore pair and biotin (Figure S1B).

After optimization of the labeling reaction *in vitro*, the labeling efficiencies of DY-547 and Cy5 reached approximately 45% and 71%, respectively, indicating that approximately 32% of molecules would be suitable for smFRET analysis using total internal reflection fluorescence (TIRF) microscopy. To assess whether the secondary structure of the capsid was disturbed by the insertion of exogenous peptides, we performed a circular dichroism assay of soluble wild-type (WT), 3XA, and 3XC capsids over the spectrum of 200–300 nm. The circular dichroism spectrum curves of 3XA and 3XC capsids were identical to that of the WT capsid (Figure 1C), indicating that the insertion of exogenous peptides in 3XA and 3XC had a negligible effect on the protein secondary structure. Using transmission electron microscopy, we also observed that the 3XA, 3XC, and labeled 3XA and 3XC proteins could self-assemble into a hexagonal VLP with a diameter of almost 17 nm (Figure 1D), similar to the PCV2 virion, indicating that the intermolecular interaction of the capsid monomers was still viable. Taken together, 3XA and 3XC capsids, with short amino acid modifications, retained the intrinsic structural features similar to the WT capsid and could also be imaged using TIRF microscopy.

Capsids Spontaneously Interconvert between Three Distinct Conformations

To disperse the capsid into monomer and minimize the disturbance of oligomerization for imaging on the TIRF microscopy, we pretreated 3XA and 3XC with imaging buffer containing NaCl at different concentrations (300 mM, 600 mM, 900 mM, 1,200 mM, 1,500 mM and 1,800 mM) for 30 min, respectively, and the pretreated samples with 1,500 mM NaCl showed the best single-molecule signals; then the capsids were immobilized on the covered quartz microscope slide in a single-molecule state (Figure S1C). We first visualized the conformational landscape of 3XA and 3XC. The smFRET trajectories of 3XA displayed a spontaneous reversible model with fluctuations between three conformations characterized by distinct FRET values of approximately 0.29, 0.48, and 0.68. Similarly, 3XC exhibited a conformational distribution with distinct FRET values of approximately 0.39, 0.59, and 0.78 (Figure 2A). Moreover, the direct transitions between the low- and high-FRET states were difficult to observe (Figure 2A), and the statistics of the transition probability also confirmed this observed phenomenon in smFRET trajectories (Figure 2B; Table S1). Both the smFRET trajectories displayed a predominant low-FRET state with a low frequency of transitions to the intermediate- and high-FRET states. The occupancy of the low-FRET state reached 77.73% $\pm$ 2.74% and 79.21% $\pm$ 0.62%, respectively, corresponding to 3XA and 3XC histograms (Figure 2C and Table S1). This was due to the higher level of off-rates from high-FRET state to intermediate-FRET state (k_{off2}) and from intermediate-FRET state to low-FRET state (k_{off1}) compared with the on-rates (k_{on1} and k_{on2}) (Figures 2D and S6). We also performed the cross check by visualizing the 3XA and 3XC labeled with cy3-maleamide and CoA-DY-647 as donor and acceptor fluorescent molecules, respectively. The results showed that 3XA and 3XC labeled with a different dye pair also mainly displayed three main states, which were similar to the 3XA and 3XC labeled with Dy-547 and Cy5 fluorescent molecules, indicating that the conformational properties/flexibility of capsid would not be affected when labeled with different dye pairs (Figures S2A and S2B). Collectively, these data demonstrated that the low-FRET state was the predominant conformation for 3XA and 3XC and that the intermediate-FRET state could be essential for the transition between low- and high-FRET states.

Binding to Heparan Sulfate Alters the Conformational Features of the Capsid

HS is the cell surface receptor for PCV2 attachment (Misinzo et al., 2006). The negative charges on the GAGs are acquired through N- and O-sulfation of the carbohydrate moieties and are crucial for their interactions (O'Donnell et al., 2010). To determine if the conformational equilibrium of the capsid changed during binding to cell receptor HS, we performed smFRET analysis of 3XA and 3XC with the addition of heparin at a saturated concentration of 2,500 μg/mL (2,200 μM, an analog of HS with a structure similar to HS's sulfated domain; the dissociation constant [K_d] between labeled 3XA and 3XC and heparin was measured to be 62 $\pm$ 4.1 μM and 71 $\pm$ 5.3 μM in the imaging buffer system, similar to the level of affinity between heparin and capsid WT [66 $\pm$ 1.4 μM]) (Figure. S5A). Compared with the smFRET data of free 3XA and 3XC, the trajectories of capsids with heparin exhibited a high-FRET-preponderant model and intermittently dropped to an intermediate state or low state for both 3XA and 3XC. The occupancy of the high-FRET state was significantly elevated to 70.30% $\pm$ 1.66% from 6.30% $\pm$ 0.34%, and the occupancy of the low-FRET state significantly decreased to 2.99% $\pm$ 0.40% from 77.73% $\pm$ 2.74% (Figures 2, 3A, and S2C; Table S1), which was due to the up-regulation of k_{on1} and k_{on2} together with the down-regulation of k_{off1} and k_{off2}

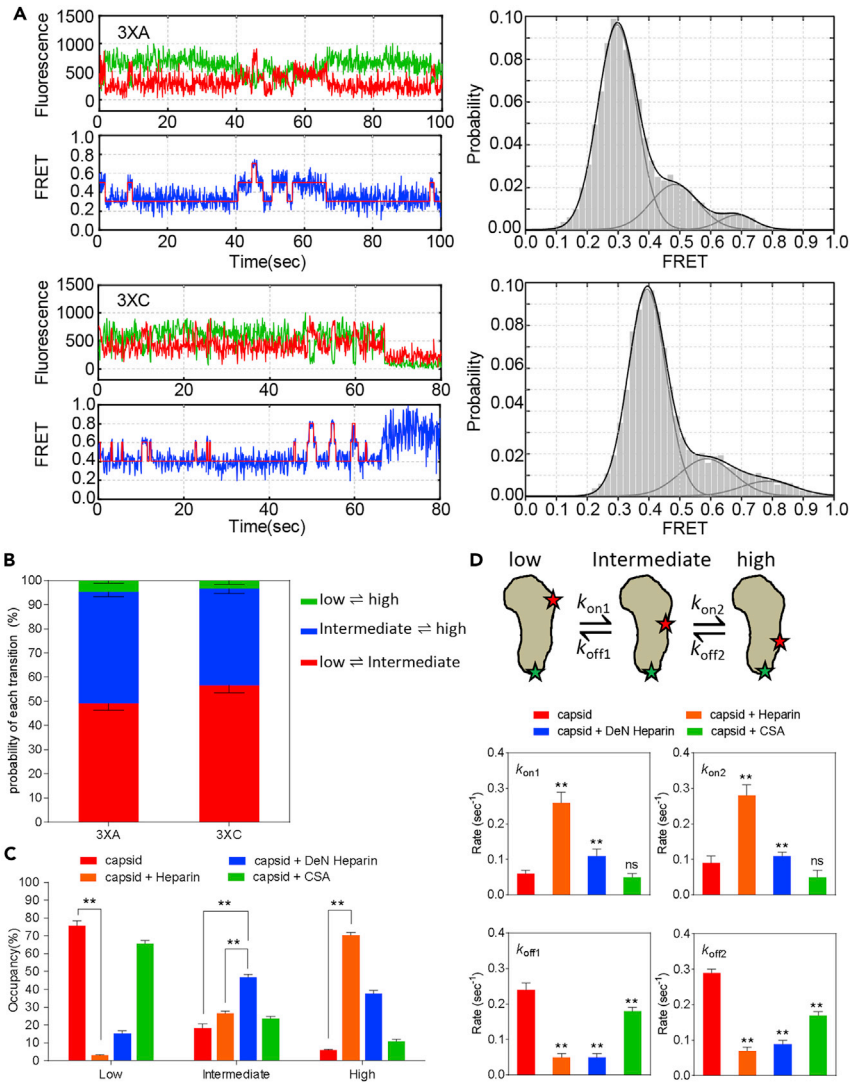

Figure 2. The Multiple Conformational Distributions of the Capsid Protein

(A) The landscapes of the capsid's conformational features. Representative fluorescence intensities of the donor and acceptor are shown as green and red, respectively, in the time trace; the original and fitted FRET values are shown as blue and red, respectively, in the FRET trajectories (left). The distinct FRET values of the main states fitted using Hidden Markov Model (HMM) were approximately 0.29, 0.48, 0.68 (3XA) and 0.39, 0.59, 0.78 (3XC), corresponding to population FRET histograms fitted with three Gaussian distributions overlaid (black) (right).

(B) Probability of transitions between smFRET states of 3XA and 3XC capsids.

(C) Occupancy of the smFRET state of 3XA data in Figures 2A and 3A–3C.

(D) The on-rates and off-rates of transitions of 3XA data in Figures 2A and 3A–3C. The results were presented as mean ± standard deviation (SD) based on three independent experiments. Significant differences between experimental and control groups were analysed using Student's t test (ns, not significant; **p < 0.01). The differences were considered significant or highly significant at p values < 0.05 and < 0.01, respectively.

(Figures 2D and S6), demonstrating that the high-FRET state is the preponderant state of the smFRET trajectory for the capsid-heparin-binding complex. Interestingly, in contrast to the capsid-heparin complexes, the mixture of capsid with a saturated concentration of 2,500 μg/mL De-N-sulfated acetylated heparin (DeN heparin, a highly sulfated HS analog without N-sulfation, 2,500 μM, $K_{d(3XA)}$ = 133 ± 3.3 μM, $K_{d(3XC)}$ = 141 ± 1.3 μM) (Figure S5B), exhibited a marked increase in the intermediate FRET state (46.98% ± 1.28%) and high-FRET state (37.73% ± 1.73%), as well as a decrease in the low-FRET state (Figures 2C, 3B, and S2D; Table S1). However, as a negative control, a mixture of capsid with a concentration of 2,500 μg/mL chondroitin sulfate A (CSA, another member of the cell surface glycosaminoglycans

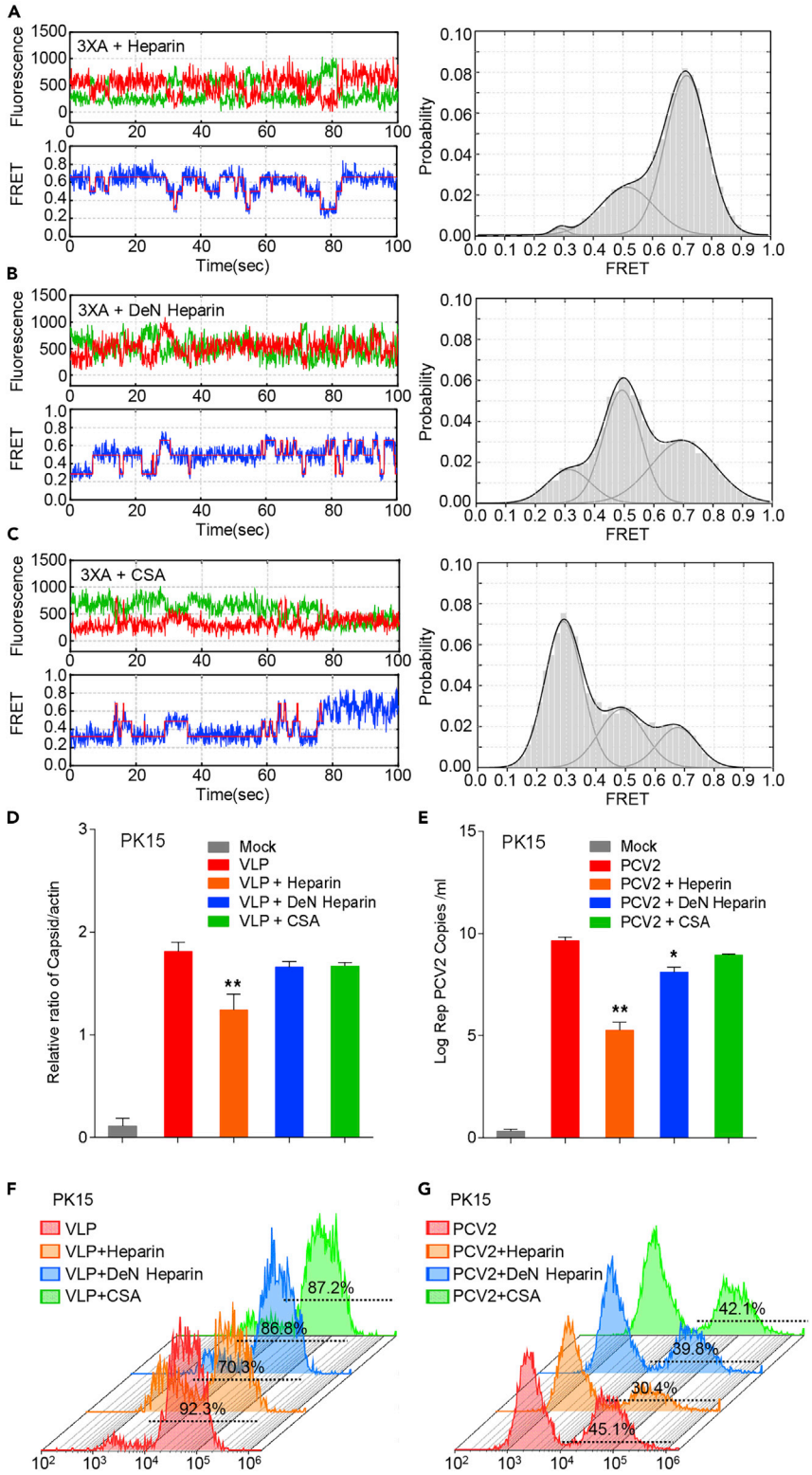

Figure 3. Interaction with Heparin Regulates the Capsid Conformational Landscape

(A–C) The histogram distribution and representative fluorescence time trace of the capsid protein's interaction with GAGs. (A) Capsid mixed with heparin. (B) Capsid mixed with De-N-sulfated acetylated heparin. (C) Capsid mixed with chondroitin sulfate A. The concentration of GAGs was fixed at 2,500 μg/mL.

Figure 3. *Continued*

(D–G) GAGs' competitive binding experiments to host cells. Equal amounts of capsid-VLPs or PCV2 virions were preincubated with heparin, De-N-sulfated acetylated heparin, and chondroitin sulfate A at 37°C for 90 min, respectively. The mixtures were then seeded onto PK15 cells for 60 min at 4°C. (D) The total amount of capsid protein bound to the cell surface was analyzed using SDS-PAGE and western blotting. (E) The number of copies of attached PCV2 virions was quantified using qPCR. (F) Capsid-VLPs bound to PK15 cells as assessed using flow cytometry. (G) PCV2 attached to PK15 cells as assessed using flow cytometry. The mean ± SD of three independent experiments was compared using Student's t-test (*$p < 0.05$; **$p < 0.01$).

See also Figures 2 and S2

but does not act as a binding receptor during the PCV2 infection, 7,100 μM, $K_{d(3XA)}$ = 478 ± 3.8 μM, $K_{d(3XC)}$ = 470 ± 8.5 μM) (Figure S5C), exhibited a similar conformational distribution to the free capsid (Figures 2, 3C, and S2E; Table S1). These findings demonstrated that the binding of negatively charged heparin altered the conformational features of the capsid and that the high-FRET state of the capsid is the main conformation during the HS interaction.

To verify whether the conformational changes in capsid affected the affinity to host cells, we performed GAGs' competitive binding experiments with PK-15 and 3D4/31 cells. The results of immunoblotting and quantitative real-time PCR assays showed that the level of bound VLPs and attached PCV2 particles to host PK15 and 3D4/31 cells with addition of soluble heparin decreased significantly compared with those of free VLPs and PCV2; however, the addition of DeN heparin or CSA had no significant effect (Figures 3D, 3E, and S2F–S2G). In addition, the flow cytometry displayed that cell adhesion of VLP and PCV2 in the presence of GAGs showed 70.3% bound VLP and 30.4% bound PCV2, which was an obvious decrease compared with free VLP and PCV2, VLP and PCV2 with added DeN heparin, or VLP and PCV2 with added CSA for PK15 cells (Figures 3F and 3G). Surprisingly, the addition of DeN heparin to VLP and PCV2 showed almost similar occupancies to those of VLP and PCV2 attached to cells compared with the CSA addition as a negative control, demonstrating that heparin without the negative charges acquired from N-sulfation is a nonfunctional HS analog for binding VLP and PCV2 virions. The results obtained using 3D4/31 cells were similar to those gained using PK15 cells (Figures S2H and S2I). In summary, soluble heparin binds to the capsid and promotes the high-FRET state, simultaneously blocking the binding of the capsid to the host cells.

Capsid-Targeting Neutralizing Antibodies Facilitate Stable Low-FRET Conformations

To investigate whether anti-capsid neutralizing monoclonal antibodies (mAbs) could block the virus binding to the cell surface by modifying the conformational transitions of the capsid, under antibody saturating condition we incubated 3XA and 3XC with the neutralizing mAbs 3F6 (2 μM, $K_{d(3XA)}$ = 0.059 ± 0.003 μM, $K_{d(3XC)}$ = 0.052 ± 0.003 μM) and 6H9 (2 μM, $K_{d(3XA)}$ = 0.134 ± 0.013 μM, $K_{d(3XC)}$ = 0.153 ± 0.028 μM) or with the non-neutralizing 8A12 (2 μM, $K_{d(3XA)}$ = 0.045 ± 0.003 μM, $K_{d(3XC)}$ = 0.053 ± 0.003 μM) and 5E11 (2 μM, $K_{d(3XA)}$ = 0.018 ± 0.002 μM, $K_{d(3XC)}$ = 0.016 ± 0.001 μM) before smFRET imaging (Figures S5F–S5I). Interestingly, the mAb 3F6 induced an absolute occupancy of the low-FRET state (94.12% ± 2.17%) and resulted in an almost compete disappearance of the intermediate-FRET and high-FRET states compared with the trajectories of the antibody-free capsid (Figures 4A and 2A). The rate analysis also displayed that k_{off1} increased most significantly, together with the decrease of k_{on1} and k_{on2}, resulting in a longer dwell time for low-FRET state, which was reflected in the capsid stabilization in the low FRET with less conformational flexibility (Figures 4C and S6). Another neutralizing mAb, 6H9, displayed similar effects to 3F6 (Figure S3A). Interestingly, although the transitions to the intermediate- and the high-FRET state were obviously suppressed, they were not completely eliminated, suggesting that the mobility of the capsid was not impaired. In contrast, the conformational distribution of the capsid treated with mAbs 8A12 or 5E11 was similar to that of the antibody-free capsid, with only a slight increase in the intermediate-FRET state, demonstrating the negligible effect of non-neutralizing mAbs in altering the antigen's conformation (Figures 4B, 2A, and S3B). Based on these results, we concluded that neutralizing antibodies could restrict the conformation of the capsid to the low-FRET state by inducing an almost complete conversion of the capsid's conformation from the intermediate- and high-FRET states to the low-FRET state without impairing the mobility of the antigen.

The Positively Charged Residues ^{99}R^{100}K within the HS-Binding Motif of the Capsid Enhance the High-FRET State during Interaction with Heparan Sulfate

The motif ^{98}IRKVKV^{103} within the capsid protein was predicted to be the binding site of HS and was located in the interior of the crystal structure of the capsid (Misinzo et al., 2006). The interaction between the GAGs

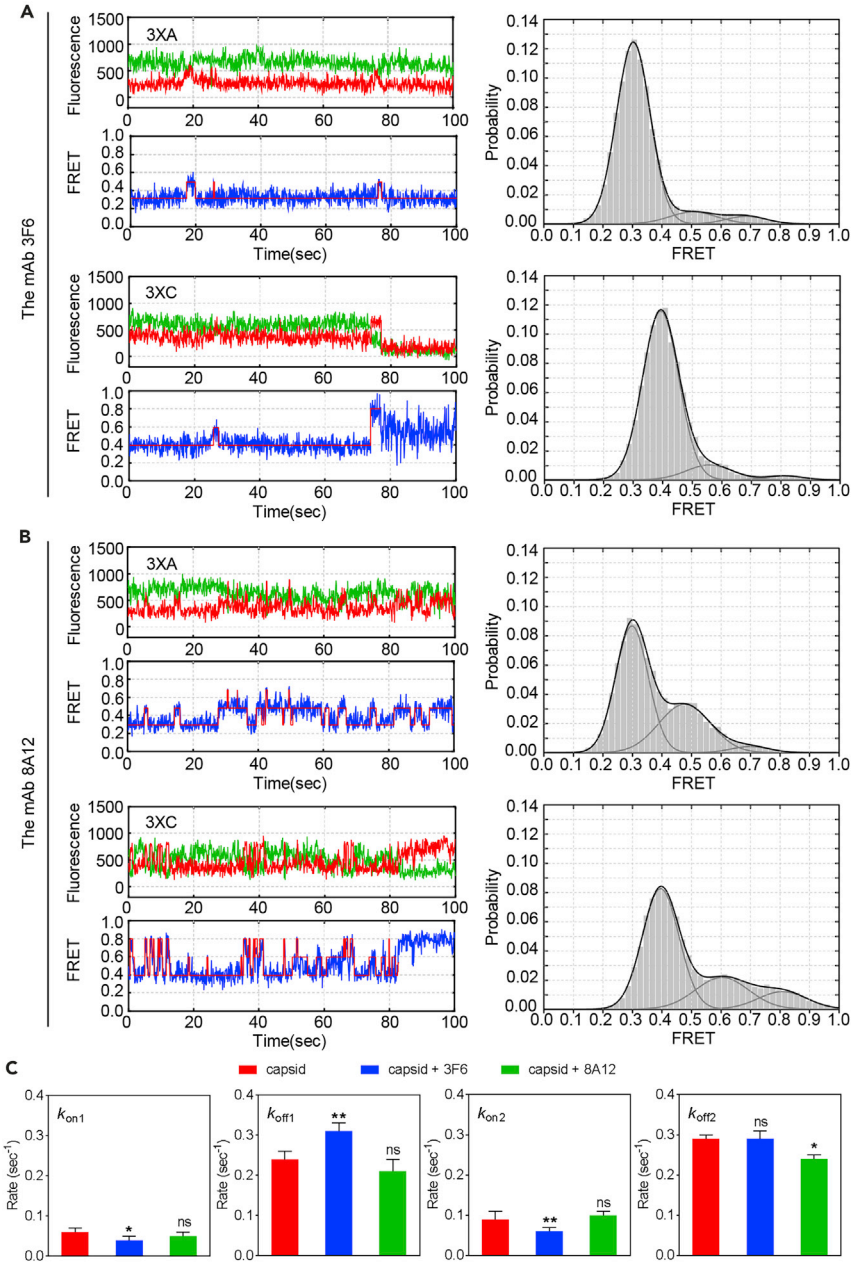

Figure 4. Neutralizing Antibodies Restrict smFRET Conformations of the Capsid Protein

Representative fluorescence time trace and histogram distribution of the anti-capsid mAbs reaction with capsids 3XA and 3XC.

(A) Capsid binding to the neutralizing mAb 3F6 reveals an absolute predominance of the low-FRET state.

(B) Capsid binding to the non-neutralizing mAb 8A12 reveals a similar conformational feature to free capsids.

(C) The on-rates and off-rates of transitions based on 3XA data in Figures 2A, 4A, and 4B. Mean ± SD of three independent experiments were shown and Student's t-test was conducted for statistical analysis (ns, not significant; *$p < 0.05$; **$p < 0.01$).

See also Figures 2 and S3

and capsid protein mainly depended on the positively charged properties of the amino acids in the binding motif (Samsonov and Pisabarro, 2016). Amino acid sequence alignment revealed that the predicted HS-binding motif ^{98}IRKVKV^{103} was highly conserved among different subtypes of PCV2 (Figure S4A). To investigate the contribution of positively charged amino acids to conformational changes during the interaction

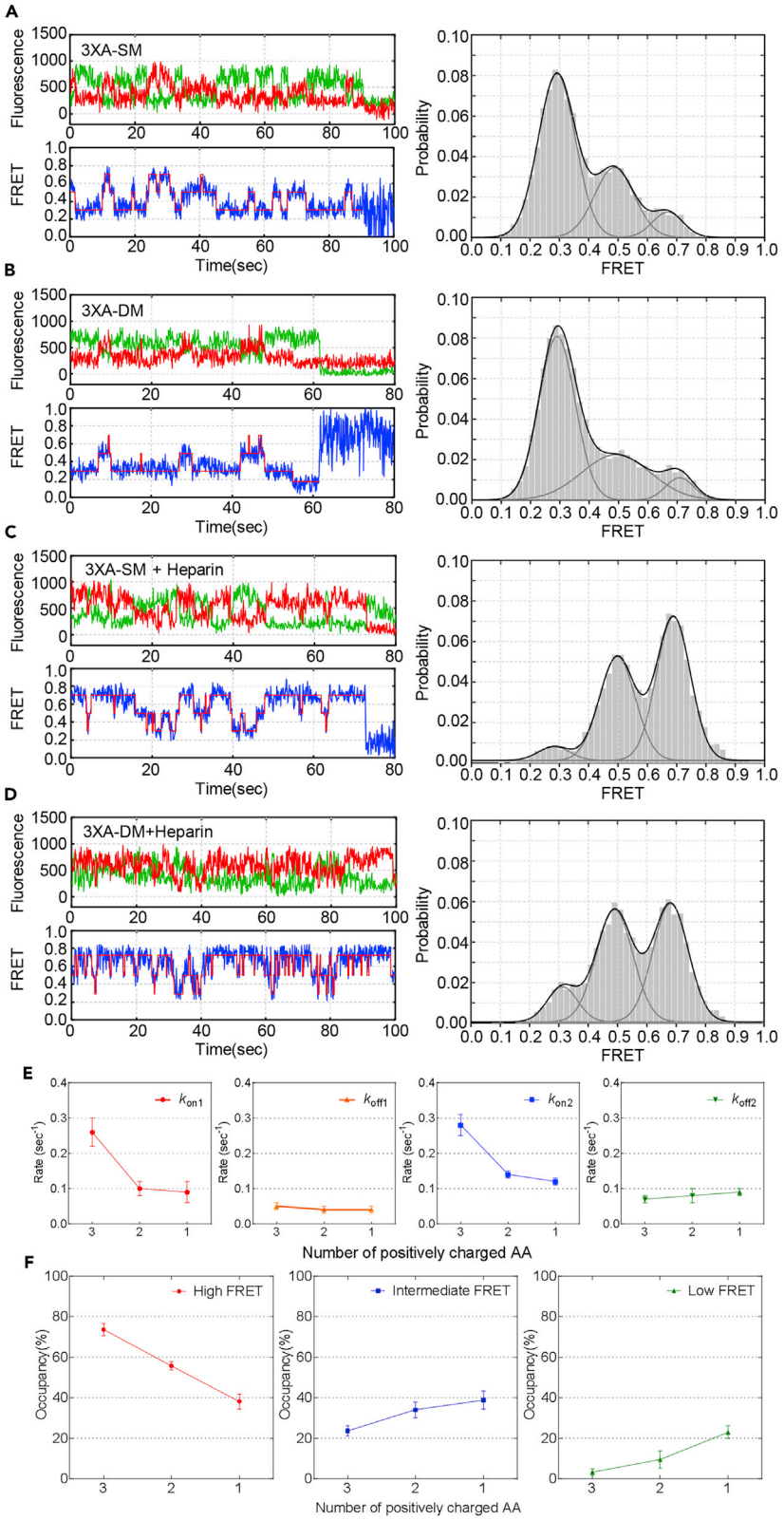
A
3XA-SM
Fluorescence
FRET
Time(sec)
Probability
FRET
B
3XA-DM
C
3XA-SM + Heparin
D
3XA-DM+Heparin
E
k_{on1}
k_{off1}
k_{on2}
k_{off2}
Rate (sec^{-1})
Number of positively charged AA
F
High FRET
Intermediate FRET
Low FRET
Occupancy(%)
Number of positively charged AA

Figure 5. Deficiency in Positively Charged Amino Acids in the Heparan Sulfate-Binding Site Alters the smFRET Conformational Feature of the Capsid Under the Effect of Heparin

(A) Conformational features of capsids-SM. The smFRET trajectory of capsid-SM showed the conformational feature of interconversion between the three intrinsic states. The histogram shows the distribution of the distinct states, similar to the landscape of capsid-WT.

(B) The smFRET trajectory and histogram of capsid-DM.

(C) Representative fluorescence trajectories and histogram distributions of capsid-SM mixed with heparin.

(D) The smFRET trajectory and histogram of capsid-DM mixed with heparin.

(E) Curve of transition rates in relation to positively charged amino acid numbers within the binding motif based on the 3XA rate data in Figure S6.

(F) Curve of each state occupancy in relation to positively charged amino acid numbers within the binding motif based on the 3XA histogram data in Figures 5A–5D. Three independent experiments were conducted. The results was presented as Mean ± SD.

See also Figure S4

with HS, we performed single-point mutation (SM) of ^{99}Arginine (R) to alanine (A), and double-point mutations (DM) of ^{99}R^{100}Lysine (K) to A within the HS-binding site of the capsid (Figure S4B). We subjected the dual-labeled capsid-SM and capsid-DM to smFRET analysis; the results displayed similar conformational dynamics to capsid-WT (Figures 2A, 5A, 5B, and S4C–S4D), such as the interconversion between the three intrinsic states and a predominant occupancy of the low-FRET state with occasional transition to intermediate and high states. This result implied that the positively charged residues ^{99}R^{110}K within the HS-binding motif did not directly regulate capsid conformational dynamics in the absence of receptor.

To further verify the role of the positively charged amino acids during the capsid's interaction with HS, we observe the smFRET landscapes of capsid-SM and capsid-DM with heparin at a saturated concentration of 2,500 μg/mL (2,200 μM) (Figures S5D and S5E). The trajectories of capsid-SM and capsid-DM still displayed the three independent states; however, the trajectories were shifted toward increased intermediate- and high-FRET states (Figures 5C, 5D, S4E and S4F). The data acquired from capsid-SM in the presence of heparin demonstrated that the occupancy of the high-FRET state was 53.76% ± 1.93%, which was significantly lower than that of capsid-WT in the presence of heparin (70.30% ± 1.66%), and the occupancies of intermediate- and low-FRET states both showed various degrees of up-regulation (Figures 5C, 3A, S2A, and S4E; Table S1). This tendency was more obvious in the mutant that lacked two positively charged amino acids in the binding motif. The trajectories of capsid-DM in the presence of heparin displayed more frequent transitions to the intermediate- and low-FRET states compared with capsid-SM and capsid-WT (Figures 5D, 3A, S2A, and S4F; Table S1), resulting in a further reduction of high-FRET state occupancy (38.12% ± 3.75%), accompanied by a slight increase in the intermediate-FRET state occupancy and increased low-FRET state occupancy. These data indicated that replacement of the positively charged amino acids within the HS-binding motif decreased the occupancy of the high-FRET state significantly during the interaction with heparin. Compared with the regulatory effect of heparin on capsid-WT, capsid-SM and capsid-DM showed slightly increased k_{off2} in the presence of heparin, indicating that the dwell time of high-FRET state was shortened, whereas the significant decrease of k_{on1} and k_{on2} suggested the longer dwell time of low and intermediate state (Figures 5E and S6). These findings hinted that capsid protein was unstable at a high-FRET state and that decreasing high-FRET occupancy correlated positively with the decreasing number of positively charged amino acids. By contrast, the occupancies of intermediate- and low-FRET states correlated negatively with the number of positively charged amino acids (Figure 5F). Taken together, these findings confirmed that the positively charged residues ^{99}R^{100}K within the HS-binding motif of the capsid were associated with the maintenance of high-FRET state during the interaction with HS.

Residues ^{99}R^{100}K of the HS-Binding Site Are Critical for the Affinity of the Capsid to the Host Cell

To further investigate the contribution of positively charged amino acid residues within the HS-binding motif of the capsid to receptor binding, we performed binding force and cell adhesion tests of capsid-SM and capsid-DM. As expected, the amount of capsid-SM and capsid-DM that bound to the HiTrap Heparin-Sepharose HP Column was significantly decreased compared with that of the capsid-WT (Figure 6A). Simultaneously, the dissociation constants (K_d) of capsid-SM (97 ± 2.4 μM) and capsid-DM (108 ± 2.4 μM) displayed an obvious increase compared with that of WT capsid (66 ± 1.4 μM) measured by microscale thermophoresis (Figures 6B and S5A). This indicated that the lack of ^{99}R^{100}K within the HS-binding motif ^{98}IRKVKV^{103} would critically impair the affinity of the capsid for heparin.

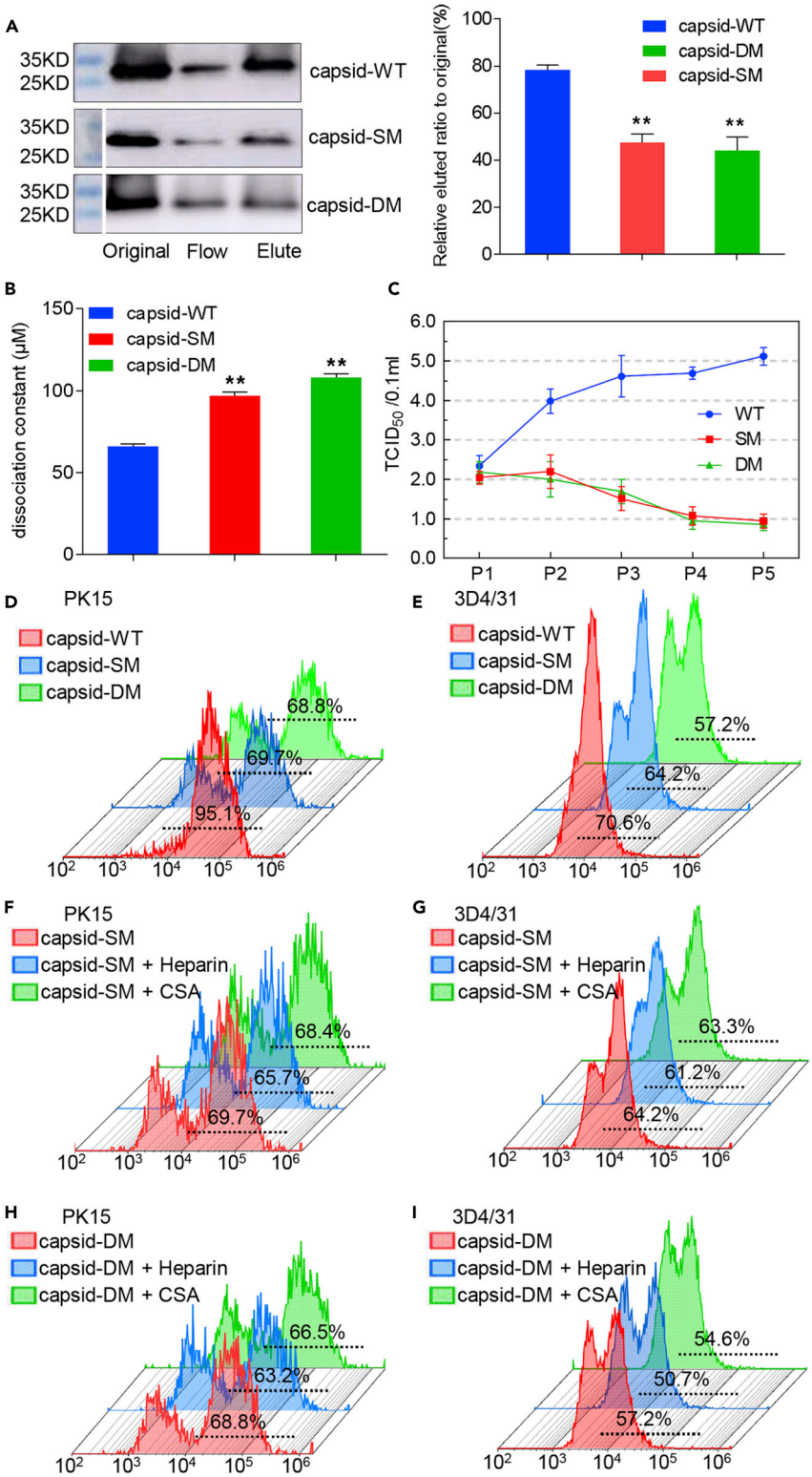
A
35KD
25KD
capsid-WT
capsid-SM
capsid-DM
Original
Flow
Elute
Relative eluted ratio to original(%)
capsid-WT
capsid-DM
capsid-SM
B
dissociation constant (μM)
C
TCID50/0.1ml
WT
SM
DM
P1
P2
P3
P4
P5
D
PK15
capsid-WT
capsid-SM
capsid-DM
68.8%
69.7%
95.1%
E
3D4/31
57.2%
64.2%
70.6%
F
PK15
capsid-SM
capsid-SM + Heparin
capsid-SM + CSA
68.4%
65.7%
69.7%
G
3D4/31
63.3%
61.2%
64.2%
H
PK15
capsid-DM
capsid-DM + Heparin
capsid-DM + CSA
66.5%
63.2%
68.8%
I
3D4/31
54.6%
50.7%
57.2%

Figure 6. The Charged Amino Acids within the Binding Site Regulate the Affinity of Capsid and Virion for the Host Cells

(A) Relative affinity of the WT, SM, and DM capsids to heparin was measured using HiTrap Heparin-Sepharose HP Column chromatography. The ratio of eluted to original amount was calculated to evaluate the relative affinity to Heparin-Sepharose of each sample. The irrelevant lanes of blot images were digitally eliminated at the position marked as space.

(B) Level of dissociation constants (K_d) between capsid-WT and mutants. The Cy5-labeled WT, SM, and DM capsids were mixed with various concentration of heparin for 15 min at room temperature, and the K_d values were determined using microscale thermophoresis.

(C) Infectivity decrease of rescued viruses with deficiency in positively charged amino acids in the binding motif. $TCID_{50}$ titration was performed according to the Reed-Muench method.

(D–I) Capsid-bound cells measured by flow cytometry. The PK15 and 3D4/31 cells were incubated with capsid-WT, capsid-SM, capsid-DM, or mixtures of capsid-SM/Heparin, capsid-DM/Heparin, capsid-SM/CSA, and capsid-DM/CSA, separately. The resultant cells were assessed by flow cytometry. (D) Capsid-positive PK15 cells, (E) capsid-positive 3D4/31 cells, (F) capsid-SM-positive PK15 cells, (G) capsid-SM-positive 3D4/31 cells, (H) capsid-DM-positive PK15 cells, and (I) capsid-DM-positive 3D4/31 cells. The mean ± SD of three independent experiments was compared using Student's t-test (**$p < 0.01$).

See also Figure S5

Given that the affinity of the capsid for heparin was weakened by the partial replacement of positively charged amino acids, we next asked whether the lack of these residues would disturb the virus life cycle. Therefore, we performed virus rescue of PCV2 with the capsid-SM and capsid-DM mutations. The self-cyclized PCV2 genomes with the ^{99}A or ^{99}A^{100}A mutation of the *capsid* gene were transfected into PK15 cells to rescue the virus, which was serially passaged to detect infectivity using the $TCID_{50}$ assay (He et al., 2013). The one-step growth curve indicated that the genomes with the capsid-SM or capsid-DM mutations could be rescued; however, the infectivity of the rescued virus was weakened compared with that of the WT virus (Figure 6C), demonstrating that the replacement of these positively charged residues within the HS-binding site of the capsid could attenuate the replication ability of PCV2. To further validate whether the weakened replication ability of PCV2 particles with capsid-SM or capsid-DM involves cell attachment, we attempted cell adhesion assays of capsid-SM or capsid-DM using flow cytometry. Flow cytometry showed that the number of adhesive cells presenting capsid-SM or capsid-DM molecules was significantly decreased compared with that of the capsid-WT (Figures 6D and 6E). However, the number of adhesive cells in the presence of HS was not significantly decreased when compared with that of free capsid-SM or capsid-DM (Figures 6F–6I), suggesting that the positive charge deficiencies in the HS-binding motif made the capsid non-sensitive to HS and reduced the cell-binding ability. Thus, these *in vivo* and *in vitro* experiments demonstrated that the positively charged residues ^{99}R^{100}K within the HS-binding motif of the capsid are critical to enhance virus attachment to the host cell surface and to regulate virus infectivity.

DISCUSSION

HS, a GAG present on the cell membrane, was identified as the cell surface receptor for various enveloped and nonenveloped viruses (Feldman et al., 2000; Meneghetti et al., 2015; Zaiss et al., 2016). In the present study, PCV2 was used as a model of nonenveloped virus, which is the smallest DNA virus that comprises one unique capsid protein, and HS was used as the receptor for attachment to host cells (Khayat et al., 2011; Misinzo et al., 2006). The direct observation of the capsid conformational changes for nonenveloped viruses has not yet been achieved because of the lack of methodology to probe such dynamics on a relevant timescale. In the present study, the usage of smFRET imaging provided the first real-time visualization of the conformational dynamics of the PCV2 capsid. The results of the present study indicated that the capsid may be regarded as a dynamic machine, undergoing spontaneous, reversible fluctuations between multiple conformations during attachment to the cell surface. Our results suggested that receptor binding regulates the intrinsic conformational dynamics of the capsid, associating with virus to invade the host cells.

The Multiple Conformations of the Capsid with Spontaneous Reversible Interconversion

The crystal structure of the PCV2 VLP revealed that the HS-binding motif ^{98}IRKVKV^{103} was deeply hidden in the interior of the VLP (Khayat et al., 2011; Misinzo et al., 2006). In the present study, Cy5 and DY-547 were labeled at ^{108}Cysteine near the HS-binding site and at the CD loop or C-terminal loop far from the HS-binding site of the capsid (Figure S1A). The smFRET approach presented a landscape in which the capsid spontaneously transited among at least three conformations, represented by the low-, intermediate-, and high-FRET states. The capsid displayed a predominantly low-FRET landscape, with transitions to the intermediate- or high-FRET states (Figure 2A). Notably, the structural proteins of enveloped viruses,

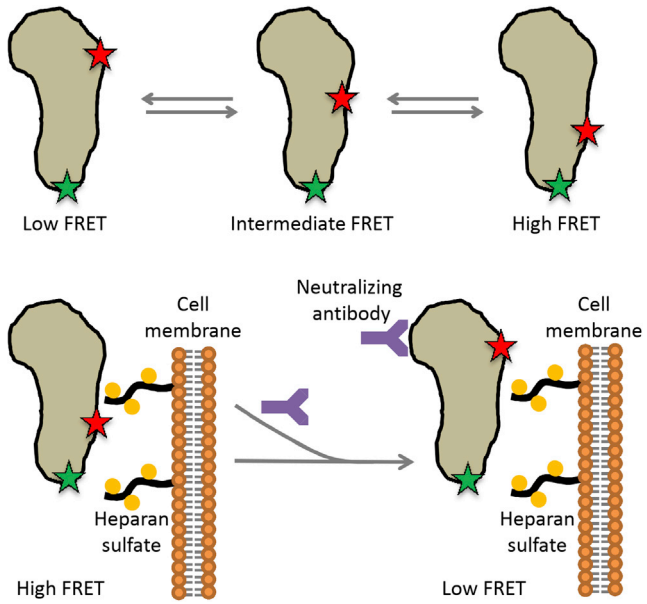

Figure 7. Model of Capsid Conformational Changes Associated with Attachment to the Cell Surface

Interaction with the receptor HS promotes the preponderance of the high-FRET state and exposes the hidden HS-binding site. By contrast, interaction with the anti-capsid neutralizing mAb results in prevention of the conformational transition and restriction to the low-FRET state, thereby blocking exposure of the HS-binding site and preventing the interaction with the cell receptor heparan sulfate.

such as glycoprotein gp120 subunit of the HIV-1 envelope trimmers (Munro et al., 2014) and hemagglutinin of influenza virus (Das et al., 2018), show similar dynamic inter-conversions between multiple distinct conformations. Thus, for the first time, we demonstrated that the capsid of a nonenveloped circovirus could spontaneously and reversibly interconvert among multiple conformations. Regrettably, current techniques limited to construct the PCV2 VLP containing only one double fluorophore-labeled capsid *in vitro*, which made it difficult to detect the conformational kinetics of the capsid in the form of icosahedral virus particles. However, in our experiments the dual fluorophore-labeled capsid monomer retained the protein secondary conformation and intermolecular forces similar to capsid-WT; we believed that the conformational features of capsid monomers was still meaningful.

GAGs and Neutralizing Antibodies Alter the Capsid's Conformational Feature

HS acts as the principal GAG receptor for the attachment of PCV2 capsid, which is partially mediated by electrostatic binding between the negatively charged chains of HS and basic amino acids within the target proteins (Bartlett and Park, 2010; Kjellen and Lindahl, 1991). Indeed, our binding experiments emphasized the superiority of HS over CSA and further demonstrated the requirement for N-sulfation of heparin for interaction with the capsid. The dynamic equilibrium of the capsid was entirely rearranged by negatively charged heparin, ultimately triggering the emergence of the high-FRET state (Figures 3A and S2A). Notably, the negative charge-deficient heparan analog DeN heparin could induce transition from the low-FRET state to the intermediate-FRET sate, but was insufficient to induce the high-FRET state (Figures 3B and S2B). However, the competitive binding assay showed that DeN heparin was incapable of binding to the capsid protein or the virus (Figures 3D–3G), indicating that the intermediate-FRET state was not an effective conformation for receptor interaction. Therefore, we hypothesized that the high-FRET state is indispensable to the efficient interaction between the capsid and the GAG receptor, and the hidden HS-binding site might be exposed on the virion surface when negatively charged HS is encountered (Figure 7). However, the current technique could not distinguish if the capsid conformational transitions occurred after the receptor binding to sustain the interaction or if the conformational transitions were induced by the receptor molecule before the binding event (Kim et al., 2013).

In contrast to the effect of HS, the capsid showed a tendency to stabilize in the low-FRET state in the presence of the anti-capsid neutralizing mAbs (Figures 4A and S3A), indicating that the neutralizing antibodies

prevented the capsid from attaching to the cell surface by restricting the conformational dynamics and consequently disrupting the interaction between the capsid and HS. Interestingly, the antigenic epitope of the capsid recognized by neutralizing mAb 3F6 is ^{156}YHSRYFT^{162}(Shang et al., 2009), but not the HS-binding site. So we hypothesized that the interaction with the neutralizing mAb prevented the conformational transitions and restricted the capsid to the low-FRET state, thereby blocking the allosteric effects that expose the HS-binding site to allow interaction with cell receptor (Figure 7). This could be considered as indirect evidence for the significance of the high-FRET state during the capsid-cell receptor interaction.

Charge Distribution of the Binding Motif Dictated the Effective Receptor-Ligand Binding

The HS-binding region formed a hydrophilic pocket wrapped around and folded over the heparin octaose moiety, producing a complementary structure for the heparin-protein interaction (Shriver et al., 2012). The key factors that produce such a hydrophilic pocket are clusters of basic amino acids distributed in the motif, especially arginine and lysine residues (Cardin and Weintraub, 1989). These clusters contribute to the formation of a center with a high positive charge density, which could interact electrostatically with the acidic groups of glycosaminoglycans (Meneghetti et al., 2015). We used mutagenesis to replace the ^{99}R or ^{100}K with alanine in the HS-binding site ^{98}IRKVKV^{103}. The mutants displayed the markedly attenuated affinity for heparin and reduced the binding capacity of the capsid to the cell (Figure 6), and subsequently impaired the infectivity of the rescued viruses. Likewise, the occurrence of the high-FRET state also decreased markedly as the number of positively charged amino acids in the binding motif decreased. Nonetheless, the conformational transition could still occur in the mutants in the presence of heparin (Figures 5C, 5D, and S4E–S4F) and the binding of the mutants was not completely abolished, indicating that the interaction could be supported by the remaining positively charged amino acid(s) within the motif or by the existence of other binding sites, such as the weak HS-binding sites on the surface of the PCV2 VLP.

Biological Significance of Conformational Feature Regulation during Virus Attachment

In this study, the high-FRET state was revealed to be the crucial configuration of capsid-HS interaction. This state reflected a distinct conformation in which the hidden HS-binding site is vicinal to the exterior area of the virus particle, allowing the capsid to establish a chemical connection with the receptor molecule on the cell surface. Besides, the existence of the intermediate-FRET state was a frequent and interesting phenomenon in all the smFRET assays. It was especially conspicuous when the capsid interacted with the electronegatively incomplete heparin and when heparin interacted with partially electropositively impaired capsid mutants, but ultimately could not accomplish the receptor-ligand interaction. Thus, the intermediate-FRET state of the capsid might be a stopover between the low-FRET state and high-FRET state. The existence and maintenance of the intermediate-FRET state could be quite meaningful and important for the biochemical events of the virus. It might prevent the conformational transition to the ultimate structure occurring too quickly when induced by an incomplete interforce and other biochemical attractive forces, thus minimizing meaningless binding to inappropriate receptors.

In this study, we demonstrated the PCV2 capsid monomer acts as a dynamic machine, spontaneously adopting multiple conformations with reversible interconversion. The intrinsic conformational features could be regulated by glycosaminoglycan receptors and neutralizing antibodies, and involved the exposure and masking of the binding site. The capsid protein is the sole structural protein of the smallest icosahedral circovirus and is a canonical glycosaminoglycan ligand; therefore the results increased our understanding of the mechanism(s) by which nonenveloped virus attach to cells. Our smFRET imaging methodology provided a platform to detect the conformational dynamics of nonenveloped viruses and will facilitate future studies of the infection mechanisms of nonenveloped viruses.

Limitations of the Study

We focused on the conformational dynamics of PCV2 capsid and revealed the regulation of the protein conformational characteristics when it bond to the cell surface receptors and neutralizing antibodies, which contributed to the further understanding of the interaction between PCV2 virions and host cells during the viral invasion. However, several limitations in this study deserved attention.

(1). Due to the technical limitations of protein fluorescent molecules' labeling method and the viral protein's self-assembly property, we could not test the capsid's conformational dynamics in the form of whole virus particles or VLPs.

(2). We presented the viral protein's allosteric effect with smFRET *in vitro*. More *in vivo* experiment techniques should be adopted to verify these conformational changes and emphasize their biological importance.

Resource Availability

Lead Contact

Further information and requests for resources should be directed to and will be fulfilled by the Lead Contact, Jinyan Gu (gujinyan@zju.edu.cn).

Materials Availability

This study did not generate new unique reagents, and all the materials involved in this study are included in the main text and Supplemental Information.

Data and Code Availability

The data that support the findings of this study are available from the corresponding author upon reasonable request.

METHODS

All methods can be found in the accompanying Transparent Methods supplemental file.

SUPPLEMENTAL INFORMATION

Supplemental Information can be found online at https://doi.org/10.1016/j.isci.2020.101547.

ACKNOWLEDGMENTS

This work was supported by grants from the National Natural Science Foundation of China (31230072) and the National Key Research and Development Program of China (2017YFD0500101). We cordially thank Dr. Fei Liu and Mr. Chengcheng Wu from Nanjing Agricultural University Institute of Immunology for operating smFRET microscopy.

AUTHOR CONTRIBUTIONS

Jiyong Zhou, J.L., and J.G. conceived the experiments. J.L. and J.G. prepared the samples and conducted most experiments. J.G., S.W., and J.L. performed immunoblotting assays and constructed the infectious clone. Jianwei Zhou, J.L., and C.L. performed the purification of virus-like particles and observation of TEM. Jiyong Zhou, J.L., J.G., F.W., and B.S. analyzed and interpreted the data. Jiyong Zhou, J.L., and J.G. wrote the manuscript.

DECLARATION OF INTERESTS

The authors declare no competing interests.

Received: October 4, 2019
Revised: February 12, 2020
Accepted: September 7, 2020
Published: October 23, 2020

REFERENCES

Allan, G.M., and Ellis, J.A. (2000). Porcine circoviruses: a review. J. Vet. Diagn. Invest. *12*, 3–14.

Bartlett, A.H., and Park, P.W. (2010). Proteoglycans in host-pathogen interactions: molecular mechanisms and therapeutic implications. Expert Rev. Mol. Med. *12*, e5.

Bernfield, M., Gotte, M., Park, P.W., Reizes, O., Fitzgerald, M.L., Lincecum, J., and Zako, M. (1999). Functions of cell surface heparan sulfate proteoglycans. Annu. Rev. Biochem. *68*, 729–777.

Cardin, A.D., and Weintraub, H.J. (1989). Molecular modeling of protein-glycosaminoglycan interactions. Arteriosclerosis *9*, 21–32.

Das, D.K., Govindan, R., Nikic-Spiegel, I., Krammer, F., Lemke, E.A., and Munro, J.B. (2018). Direct visualization of the conformational dynamics of single influenza hemagglutinin trimers. Cell *174*, 926–937 e912.

Dennis, T.P.W., Flynn, P.J., de Souza, W.M., Singer, J.B., Moreau, C.S., Wilson, S.J., and Gifford, R.J. (2018). Insights into circovirus host range from the genomic fossil record. J. Virol. *92*, e00145-18.

Fairhead, M., and Howarth, M. (2015). Site-specific biotinylation of purified proteins using BirA. Methods Mol. Biol. *1266*, 171–184.

Feldman, S.A., Audet, S., and Beeler, J.A. (2000). The fusion glycoprotein of human respiratory syncytial virus facilitates virus attachment and infectivity via an interaction with cellular heparan sulfate. J. Virol. *74*, 6442–6447.

Finsterbusch, T., and Mankertz, A. (2009). Porcine circoviruses–small but powerful. Virus Res. *143*, 177–183.

Ha, T. (2001). Single-molecule fluorescence resonance energy transfer. Methods *25*, 78–86.

Ha, T., Enderle, T., Ogletree, D.F., Chemla, D.S., Selvin, P.R., and Weiss, S. (1996). Probing the interaction between two single molecules: fluorescence resonance energy transfer between a single donor and a single acceptor. Proc. Natl. Acad. Sci. U S A *93*, 6264–6268.

He, J., Cao, J., Zhou, N., Jin, Y., Wu, J., and Zhou, J. (2013). Identification and functional analysis of the novel ORF4 protein encoded by porcine circovirus type 2. J. Virol. *87*, 1420–1429.

Huan, C.C., Wang, Y., Ni, B., Wang, R., Huang, L., Ren, X.F., Tong, G.Z., Ding, C., Fan, H.J., and Mao, X. (2015). Porcine epidemic diarrhea virus uses cell-surface heparan sulfate as an attachment factor. Arch. Virol. *160*, 1621–1628.

Joyce, J.G., Tung, J.S., Przysiecki, C.T., Cook, J.C., Lehman, E.D., Sands, J.A., Jansen, K.U., and Keller, P.M. (1999). The L1 major capsid protein of human papillomavirus type 11 recombinant virus-like particles interacts with heparin and cell-surface glycosaminoglycans on human keratinocytes. J. Biol. Chem. *274*, 5810–5822.

Khayat, R., Brunn, N., Speir, J.A., Hardham, J.M., Ankenbauer, R.G., Schneemann, A., and Johnson, J.E. (2011). The 2.3-angstrom structure of porcine circovirus 2. J. Virol. *85*, 7856–7862.

Kim, E., Lee, S., Jeon, A., Choi, J.M., Lee, H.S., Hohng, S., and Kim, H.S. (2013). A single-molecule dissection of ligand binding to a protein with intrinsic dynamics. Nat. Chem. Biol. *9*, 313–318.

Kjellen, L., and Lindahl, U. (1991). Proteoglycans: structures and interactions. Annu. Rev. Biochem. *60*, 443–475.

Li, J.P., and Spillmann, D. (2012). Heparan sulfate proteoglycans as multifunctional cell regulators: cell surface receptors. Methods Mol. Biol. *836*, 239–255.

Liu, Z., Guo, F., Wang, F., Li, T.C., and Jiang, W. (2016). 2.9 A resolution cryo-EM 3D reconstruction of close-packed virus particles. Structure *24*, 319–328.

Mahe, D., Blanchard, P., Truong, C., Arnauld, C., Le Cann, P., Cariolet, R., Madec, F., Albina, E., and Jestin, A. (2000). Differential recognition of ORF2 protein from type 1 and type 2 porcine circoviruses and identification of immunorelevant epitopes. J. Gen. Virol. *81*, 1815–1824.

Meneghetti, M.C., Hughes, A.J., Rudd, T.R., Nader, H.B., Powell, A.K., Yates, E.A., and Lima, M.A. (2015). Heparan sulfate and heparin interactions with proteins. J. R. Soc. Interf. *12*, 0589.

Michalet, X., Weiss, S., and Jager, M. (2006). Single-molecule fluorescence studies of protein folding and conformational dynamics. Chem. Rev. *106*, 1785–1813.

Misinzo, G., Delputte, P.L., Meerts, P., Lefebvre, D.J., and Nauwynck, H.J. (2006). Porcine circovirus 2 uses heparan sulfate and chondroitin sulfate B glycosaminoglycans as receptors for its attachment to host cells. J. Virol. *80*, 3487–3494.

Munro, J.B., Gorman, J., Ma, X., Zhou, Z., Arthos, J., Burton, D.R., Koff, W.C., Courter, J.R., Smith, A.B., 3rd, Kwong, P.D., et al. (2014). Conformational dynamics of single HIV-1 envelope trimers on the surface of native virions. Science *346*, 759–763.

Nawagitgul, P., Morozov, I., Bolin, S.R., Harms, P.A., Sorden, S.D., and Paul, P.S. (2000). Open reading frame 2 of porcine circovirus type 2 encodes a major capsid protein. J. Gen. Virol. *81*, 2281–2287.

O'Donnell, C.D., Kovacs, M., Akhtar, J., Valyi-Nagy, T., and Shukla, D. (2010). Expanding the role of 3-O sulfated heparan sulfate in herpes simplex virus type-1 entry. Virology *397*, 389–398.

Prydz, K., and Dalen, K.T. (2000). Synthesis and sorting of proteoglycans. J. Cell Sci. *113 Pt 2*, 193–205.

Rostand, K.S., and Esko, J.D. (1997). Microbial adherence to and invasion through proteoglycans. Infect. Immun. *65*, 1–8.

Roy, R., Hohng, S., and Ha, T. (2008). A practical guide to single-molecule FRET. Nat. Methods *5*, 507–516.

Samsonov, S.A., and Pisabarro, M.T. (2016). Computational analysis of interactions in structurally available protein-glycosaminoglycan complexes. Glycobiology *26*, 850–861.

Sarrazin, S., Lamanna, W.C., and Esko, J.D. (2011). Heparan sulfate proteoglycans. Cold Spring Harb. Perspect. Biol. *3*, a004952.

Sasaki, M., Anindita, P.D., Ito, N., Sugiyama, M., Carr, M., Fukuhara, H., Ose, T., Maenaka, K.,

Takada, A., Hall, W.W., et al. (2018). The role of heparan sulfate proteoglycans as an attachment factor for rabies virus entry and infection. J. Infect. Dis. *217*, 1740–1749.

Shang, S.B., Jin, Y.L., Jiang, X.T., Zhou, J.Y., Zhang, X., Xing, G., He, J.L., and Yan, Y. (2009). Fine mapping of antigenic epitopes on capsid proteins of porcine circovirus, and antigenic phenotype of porcine circovirus type 2. Mol. Immunol. *46*, 327–334.

Shriver, Z., Capila, I., Venkataraman, G., and Sasisekharan, R. (2012). Heparin and heparan sulfate: analyzing structure and microheterogeneity. Handb. Exp. Pharmacol. *207*, 159–176.

Tan, C.W., Poh, C.L., Sam, I.C., and Chan, Y.F. (2013). Enterovirus 71 uses cell surface heparan sulfate glycosaminoglycan as an attachment receptor. J. Virol. *87*, 611–620.

Wang, D., Zhang, S., Zou, Y., Yu, W., Jiang, Y., Zhan, Y., Wang, N., Dong, Y., and Yang, Y. (2018). Structure-based design of porcine circovirus type 2 chimeric VLPs (cVLPs) displays foreign peptides on the capsid surface. Front. Cell. Infect. Microbiol. *8*, 232.

Wang, N., Zhan, Y., Wang, A., Zhang, L., Khayat, R., and Yang, Y. (2016). In silico analysis of surface structure variation of PCV2 capsid resulting from loop mutations of its capsid protein (Cap). J. Gen. Virol. *97*, 3331–3344.

Xu, Y., Martinez, P., Seron, K., Luo, G., Allain, F., Dubuisson, J., and Belouzard, S. (2015). Characterization of hepatitis C virus interaction with heparan sulfate proteoglycans. J. Virol. *89*, 3846–3858.

Zaiss, A.K., Foley, E.M., Lawrence, R., Schneider, L.S., Hoveida, H., Secrest, P., Catapang, A.B., Yamaguchi, Y., Alemany, R., Shayakhmetov, D.M., et al. (2016). Hepatocyte heparan sulfate is required for adeno-associated virus 2 but dispensable for adenovirus 5 liver transduction in vivo. J. Virol. *90*, 412–420.

Zautner, A.E., Jahn, B., Hammerschmidt, E., Wutzler, P., and Schmidtke, M. (2006). N- and 6-O-sulfated heparan sulfates mediate internalization of coxsackievirus B3 variant PD into CHO-K1 cells. J. Virol. *80*, 6629–6636.

Zhou, Z., Cironi, P., Lin, A.J., Xu, Y., Hrvatin, S., Golan, D.E., Silver, P.A., Walsh, C.T., and Yin, J. (2007). Genetically encoded short peptide tags for orthogonal protein labeling by Sfp and AcpS phosphopantetheinyl transferases. ACS Chem. Biol. *2*, 337–346.

iScience, Volume *23*

Supplemental Information

Conformational Dynamics of Nonenveloped Circovirus Capsid to the Host Cell Receptor

Jiarong Li, Jinyan Gu, Cui Lin, Jianwei Zhou, Shengnan Wang, Jin Lei, Fengcai Wen, Bo Sun, and Jiyong Zhou

Supplemental Figures

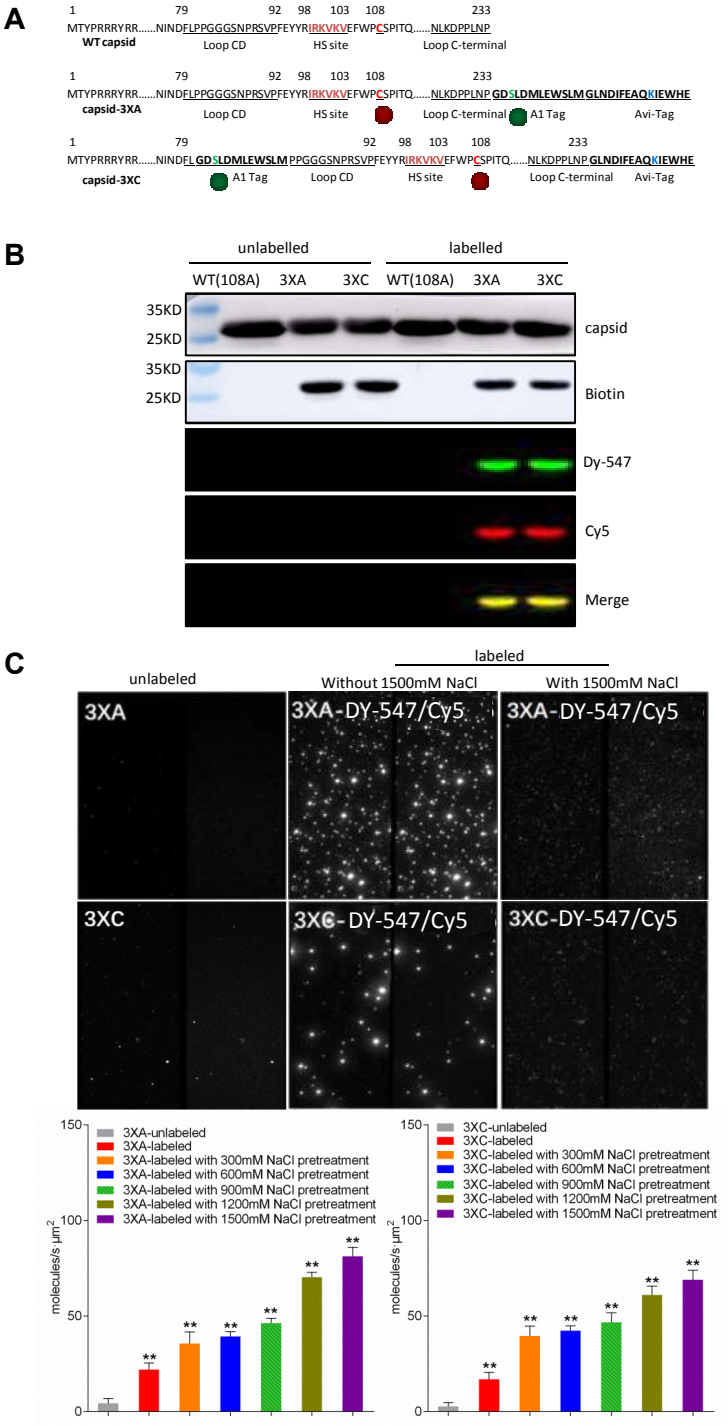

Figure S1. Strategy for Site-specific Attachment of the Donor & Acceptor Fluorophore Pair. Related to Figure 1.

(A) Schematic of the engineered capsid 3XA and 3XC, based on the WT capsid sequence of the PCV2 HZ0201 isolate. The putative heparin binding motif ^{98}IRKVKV^{103} is highlighted in crimson. ^{108}cysteine is highlighted in red and labeled by Cy5 (red ball). The A1-tag peptide (GDSLDMLEWSLM) was inserted at the C-terminus (3XA) or between the ^{80}Leucine and ^{81}Proline residues (3XC) to attached DY-547 (green ball). The Avi-tag peptide (GLNDIFEAQKIEWHE) was added at the C-terminus for the adhesion of D-biotin.

(B) Western blotting assay of Cy5/ DY-547 labeled capsid-3XA and capsid-3XC. DY-547 and Cy5 were excited by lasers at 520 nm and 630 nm, respectively. The conjugated biotin was identified using HRP-streptavidin.

(C) Capsids were subjected to the fluorescent labeling reaction, surface immobilized, and imaged using TRIF. The donor and acceptor channels view of the passivated slides immobilized with unlabeled capsid 3XA or 3XC (left); with labeled capsid 3XA or 3XC (middle); or with labeled capsid 3XA or 3XC pretreated with 1,500 mM NaCl imaging buffer for 30 min to eliminate oligomerization (right).

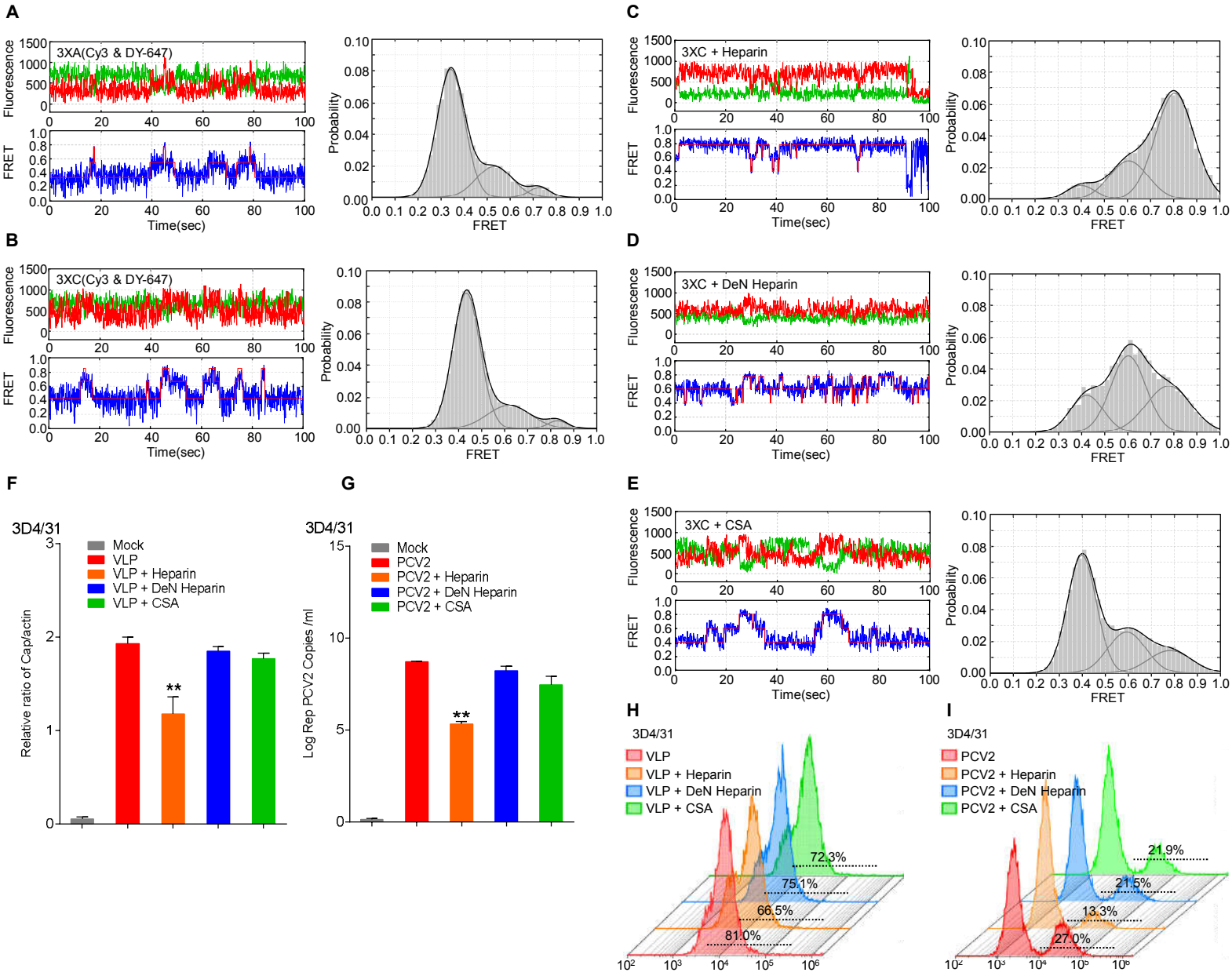

Figure S2. Interaction with Heparin Induced the High-FRET Conformation of Capsid. Related to Figure 3.

(A-B) Representative fluorescence time trace and histogram distribution of the capsid 3XA and 3XC labeled with Cy3-maleamide and CoA-Dy-647.(C-E) Typical capsid-3XC fluorescence time trace and the histogram distribution with exogenous soluble GAGs. C, capsid-3XC mixed with heparin. D, capsid-3XC mixed with De-N-sulfated acetylated heparin. E, capsid-3XC mixed with chondroitin sulfate A. The concentration of GAGs was fixed at 2,500 μg/ml.

(F-I) Competitive binding assay of VLPs and PCV2 particles for 3D4/31 cells. The experimental protocol is identical to that detailed in Figure 3. (F) Western blotting analysis of VLPs bound to soluble GAGs. (G) qPCR assay of PCV2 virions bound with soluble GAGs. H, percentage of VLPs bound to 3D4/31 cells, as assessed using flow cytometry.(I) Percentage of PCV2 bound to 3D4/31 cells, as measured using flow cytometry.

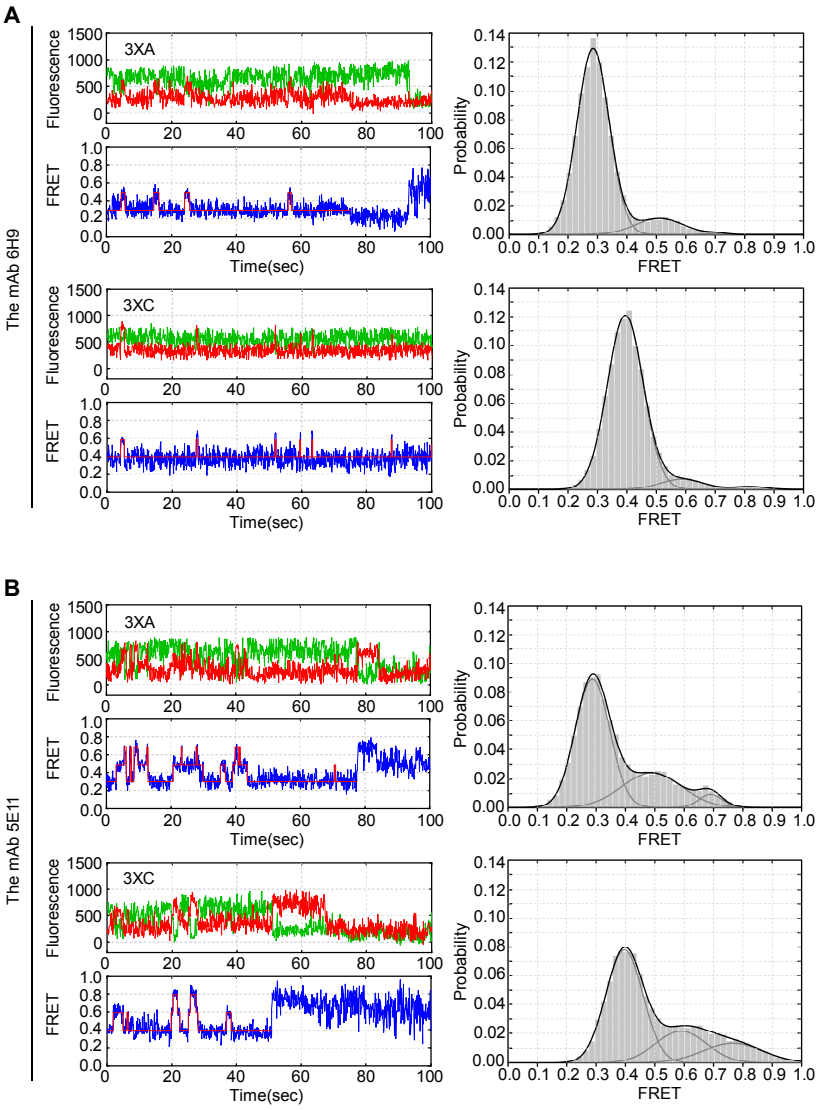

Figure S3. The Conformational Landscapes of Capsids Treated with Anti-capsid Antibodies. Related to Figure 4.

The typical fluorescence time trace and histogram distribution of capsid 3XA and 3XC reacting with mAbs.

(A) Capsids treated with neutralizing mAb 6H9 reveal an absolute predominance of the low-FRET state.

(B) Capsids treated with non-neutralizing mAb 5E11 display a similar conformational distribution to free capsids

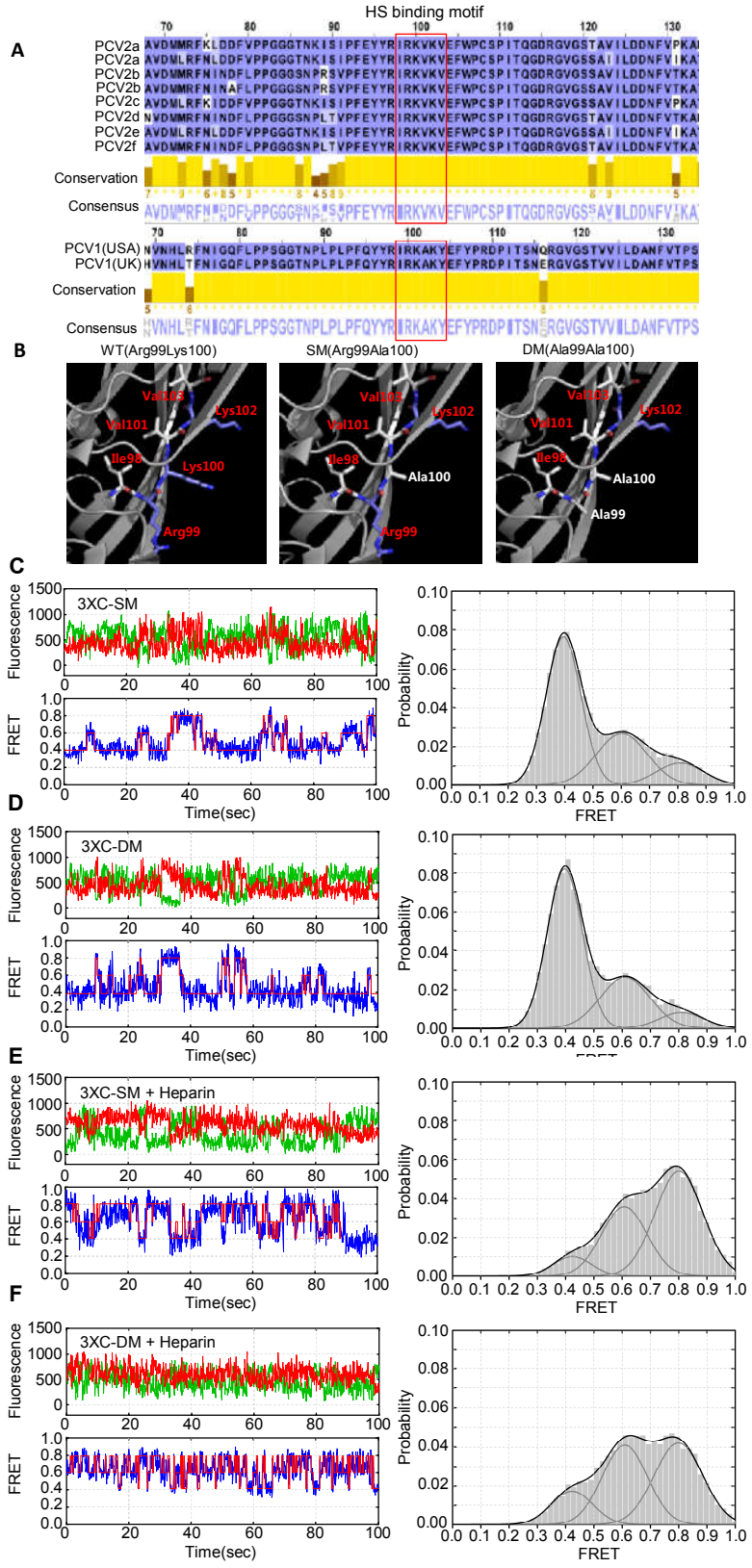

Figure S4. Deficiency of Positively Charged Amino Acids of the Binding Site Affects the Affinity to Heparin. Related to Figure 5.

(A) Conservation of putative heparin sulfate binding motif in capsid. All the amino acid sequence data were obtained from GenBank. Location and sequence of canonical putative heparin sulfate binding motif was highlighted wit a red frame.

(B) Schematic of the predicted local structure of the heparan binding site in the positively charged amino acid deficient mutants. The positively charged amino acids are labeled in blue and the uncharged amino acids are labeled in white. Left, the abundant side chain powered by the basic amino acids in capsid-WT. Middle, the side chain was reduced because of the $K^{100}A$ mutation in capsid-SM. Right, the side chain was reduced because of the $^{99}R^{100}K$ to $^{99}A^{100}A$ mutations in capsid-DM. This local structural prediction was performed on the basis of the revealed capsid structure (PDB:3R0R) and presented using the PyMOL software.

(C-D) Typical smFRET trajectories and histogram distributions of capsid-3XC- SM (C) and DM (D). Conformational features of the positively charged amino acids deficiency mutants are similar to those of free capsid-WT.

(E-F) Representative capsid-3XC fluorescence time trace and the histogram distribution of capsid-SM (E) and capsid-DM (F) with added exogenous heparin.

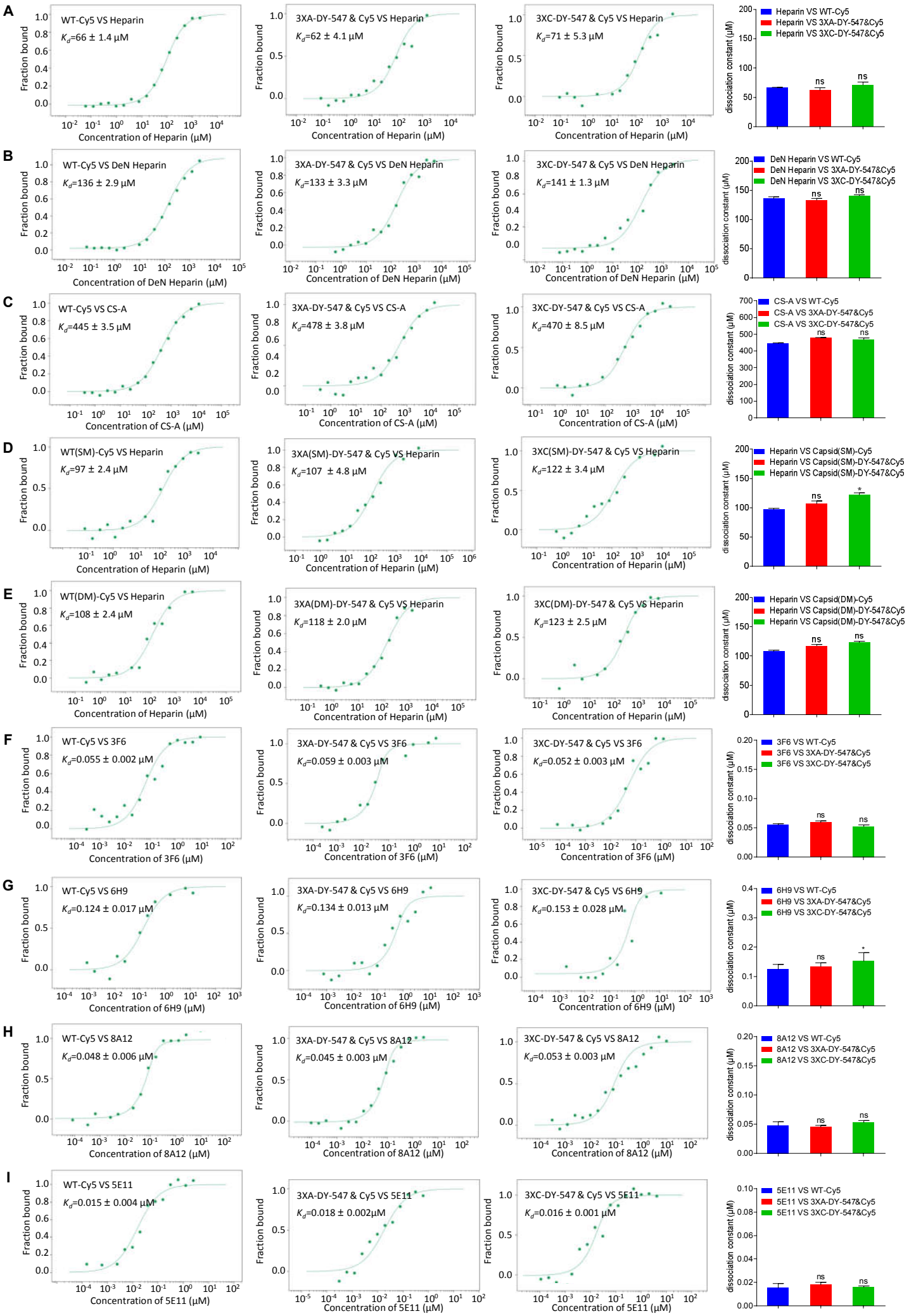

Figure S5. The dissociation constants (K_d) between the capsids and GAGs or antibodies. Related to Figure 6.

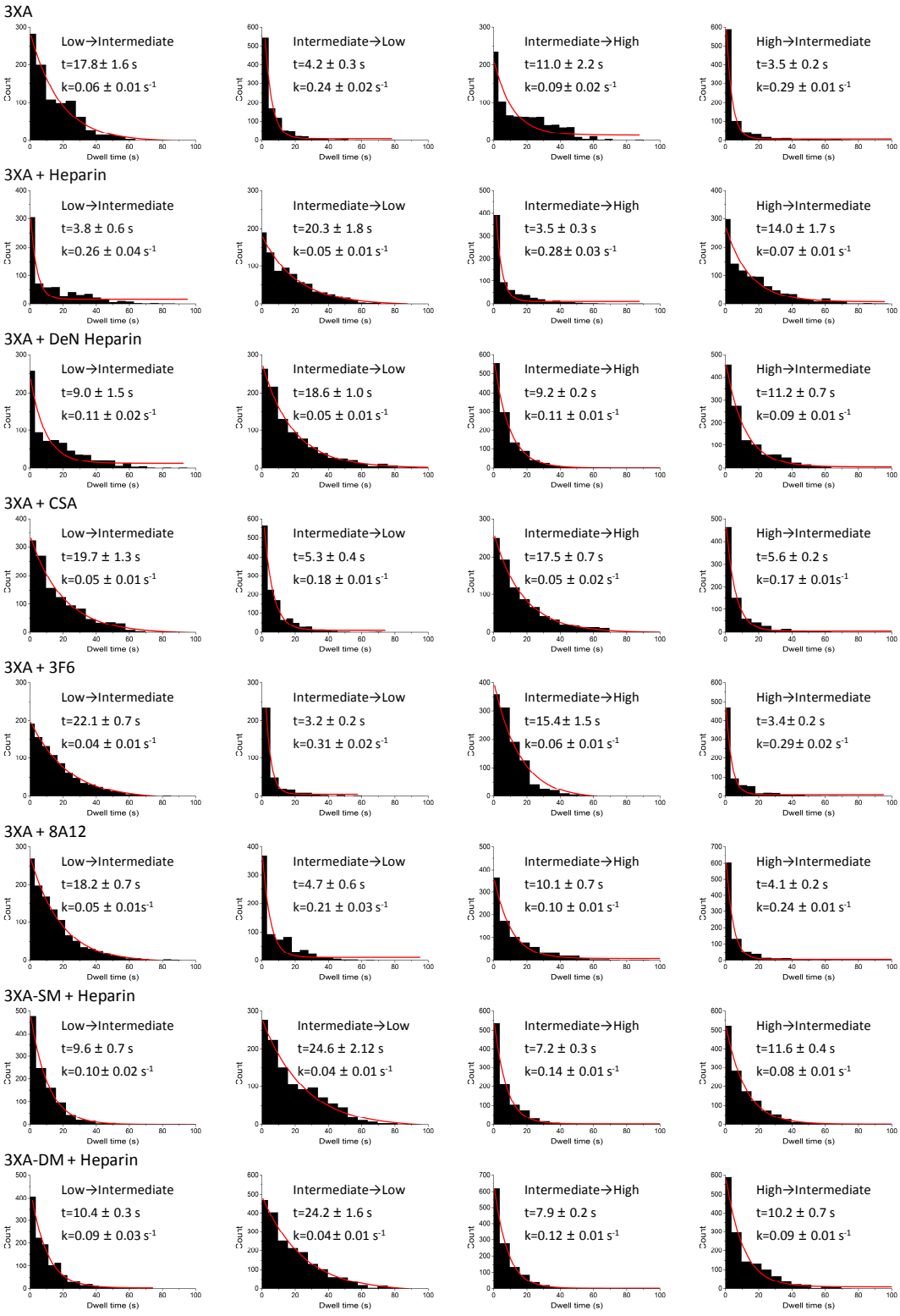

Figure S6. Dwell times and transition rates fitted from single-exponential decay curve of the 3XA smFRET experimental groups.
Related to Figure 2, 4, 5.

Supplemental Tables

Group	number of molecules	total measurement time (s)	number of transitions			state occupancy (%)		
			L⇌I	I⇌H	L⇌H	Low	Intermediate	High
3XA	103	4386.9	2127	1813	182	77.73±2.74	18.27±2.55	6.30±0.34
3XA+Heparin	115	4856.7	1349	1895	109	2.99±0.40	26.70±1.27	70.30±1.66
3XA+DeN Heparin	177	6613.3	1732	2394	164	15.29±1.47	46.98±1.28	37.73±1.73
3XA+CSA	96	3949.9	2532	1648	118	65.55±1.73	23.65±1.03	10.80±1.13
3XA+3F6	143	5587.3	1613	1539	91	94.12±2.17	4.72±1.13	1.12±0.36
3XA+8A12	101	4601.3	1747	1584	121	72.67±1.64	23.12±1.48	4.03±1.36
3XA+6H9	125	5711.6	1865	1697	137	92.57±1.63	6.32±1.06	0.73±0.23
3XA+5E11	89	4051.6	1575	1283	114	71.43±3.14	20.63±2.37	7.14±2,32
3XA-SM	77	3797.3	1437	993	78	69.12±3.17	24.56±1.83	9.13±1.43
3XA-SM+ Heparin	159	6992.2	2303	2285	363	9.47±4.14	33.94±3.85	53.76±1.93
3XA-DM	91	4256.5	1932	1362	97	72.07±3.26	18.15±2.11	8.67±0.91
3XA-DM+ Heparin	131	5830.5	2158	2917	272	22.96±3.09	38.78±4.49	38.12±3.75
3XC	122	5223.7	2972	2218	283	79.21±0.62	16.87±1.71	4.04±2.64
3XC+ Heparin	99	4304.5	1065	1673	101	1.87±1.13	21.44±2.21	77.06±3.39
3XC+DeN Heparin	141	5917.4	2565	2987	396	18.04±3.27	41.63±4.73	41.73±3.84
3XC+CSA	105	4685.5	3656	1437	158	64.33±2.47	27.73±1.83	7.35±2.73
3XC+3F6	130	5598.1	2673	1473	191	91.46±1.32	7.36±1.73	0.88±0.46
3XC+8A12	110	5670.2	1627	1334	196	70.43±2.86	23.74±3.73	13.63±2.02
3XC+6H9	162	5268.4	1935	1673	148	90.34±2.34	7.63±1.74	1.44±073
3XC+5E11	85	4624.6	1563	1143	95	65.73±2.18	17.23±2.22	16.61±1,72
3XC-SM	111	5407.1	2537	1563	161	68.62±2.38	21.14±1.12	11.46±1.23
3XC-SM+ Heparin	157	5937.9	2710	3160	293	6.54±3.08	36.34±1.26	55.73±2.12
3XC-DM	133	6701.2	1919	1453	155	72.03±3.18	16.55±1.61	10.87±1.99
3XC-DM+ Heparin	109	5022.1	1960	2563	183	23.96±2.09	37.78±1.58	38.12±1.91

Table S1. Statistics of total traces numbers, total measurement time, transitions numbers, state occupancy of smFRET groups. Related to Figure 2, 3, 4, 5.

Transparent Methods

Cell and Virus Infection

PCV-free PK15 cells and 3D4/31 cells were cultured in Opti-MEM (Gibco) and RPMI-1640 medium (Gibco), respectively. Both media were supplemented with 10% Fetal Bovine Serum (Gibco). PCV2 strain HZ0201 ($10^{5.5}TCID_{50}$/ml) was propagated in PK15 cells (Zhou et al., 2006). For the soluble GAGs competitive binding experiments, the PCV2 virions were enriched using ultra-centrifugation.

Protein Purification and Fluorophore Labeling

The *capsid* gene was obtained from the whole genome of PCV2 strain HZ0201. The A1 peptide (Figure S1A) was inserted into the CD loop or the C-terminal loop of the capsid for DY-547 fluorophore labeling, catalyzed by ACPs according to the design of the 3XA and 3XC capsids (Zhou et al., 2007). The BirA gene, encoding the biotin acceptor Avi-tag peptide (Figure S1A), was attached at the 3'-terminus of the *capsid* gene for biotinylation (Fairhead and Howarth, 2015). The engineered *capsid* gene in plasmid pET28a (Novagen) encoded a hexahistidine tag at the N-terminus. To construct the putative HS binding motif mutants of the capsid proteins with different numbers of positively charged amino acids, the ^{99}R and ^{99}R^{100}K residues were mutated to A, and the resultant capsid mutants were named capsid-SM and capsid-DM, respectively. Newly constructed vectors were transformed into Escherichia coli BL21 (DE3) and protein expression was induced using 1 mM isopropyl b-D-1-thiogalactopyranoside and 100 mM D-biotin(Millipore) at 16 ° C overnight. Biotinylated proteins were purified using an Ni-NTA super-flow matrix (Qiagen), followed by PD10 column(GE healthcare) desalting to remove the excess imidazole. The protein concentration was measured using the BCA method, followed storage at −80 ° C.

Purified proteins were dissolved in labeling buffer (50 mM HEPES, 10 mM $MgCl_2$, 10 mM $CaCl_2$, 150 mM NaCl, pH 7.5) and labeled with Cy5-maleimide (GE healthcare) and coenzyme A (CoA)-DY-547 (New England Biolabs). The proteins were preincubated with a 50-fold molar excess of Tris (2-carboxyethyl) phosphine to reduce the inter-molecular disulfide bond for 30 min at room temperature. The proteins were then mixed with 10-fold molar excess CoA- DY-547 dyes and 5 μM ACPS enzyme at 37 ° C for 90 min, followed by mixing

with a 20-fold molar excess of Cy5-maleimide at room temperature overnight (Roy et al., 2008; Zhou et al., 2007). Dual-labeled capsid proteins were separated from the unreacted excess dyes and enzymes using a PD Mini-Trap G-25 desalting column (GE healthcare) with smFRET imaging buffer (50 mM Tris, 150 mM NaCl, 1 mM Trolox, 0.8% glucose (w/v), 0.8% glucose oxidase (w/v), 0.8% catalase (w/v), pH 7.5). The anti-capsid mAb 5E11 and horseradish peroxidase-streptavidin were used for immunoblotting, and the donor and acceptor fluorophores were excited using lasers at 520 nm and 630 nm using the GE Amersham™ Typhoon NIR system to ensure the biotin and the two fluorophores were labeled in the same protein sample (Fig S1B). The donor and accepter fluorophore labeling efficiency was then calculated from the protein concentration data measured using BCA quantification and the fluorescence molecule concentration estimated based on Lambert-Beer equation with the absorbance at 550 & 630 nm. Finally the sample was stored at −80 ° C until use.

Circular Dichroism Spectrum Analysis

Purified WT, 3XA, and 3XC capsids were measured using a Chirascan™-Circular Dichroism (CD) Spectrometer (Applied Photophysics) with a path length of 0.1 mm. The CD spectra of the capsids were acquired between 200 and 300 nm with a 1-nm increment, and the spectrum of the free buffer solution was subtracted as background.

Self-assembly of PCV2 Virus-like Particles

Purified WT, 3XA, and 3XC and dual fluorophores labeled 3XA and 3XC capsids were dialyzed in the assembly buffer (NaH_2PO_4 0.1 M, Na_2HPO_4 0.1 M, Imidazole 20 mM, Tris base 0.01 M, NaCl 0.15 M, KCl 0.05 M, $MgCl_2$ 0.002 M, ammonium 0.1 M, glycerol 5%, Triton-X100 0.5%, β-mercaptoethanol 5 mM, and PMSF 0.1 mM, PH 7.6) at 4 ° C overnight. The mixture was then subjected to size-exclusion chromatography using an ÄKTA Purifier UPC 100 system (GE Healthcare) equipped with a prepacked HiPrep™ 16/60 Sephacryl™ S-300 HR column (GE Healthcare) in assembly buffer. The fractions were collected, and detected using SDS-PAGE and immunoblotting. The formation of PCV2 VLPs was observed using transmission electron microscopy (H-7650 TEM, Hitachi-Science &Technology, Japan).

Single-molecule FRET Assay

The smFRET experiment was performed based on a custom-built prism-based total internal reflection fluorescence (TIRF) microscopy method (Olympus IX81 microscope, Photometric Evolve 512 EMCCD, 50 mW, Coherent 532 nm solid-state laser). 10 μM of dual fluorophores-labeled and biotinylated protein sample was immobilized on a PEG-passivated, streptavidin-coated, quartz microscope slide through streptavidin-biotin binding for the smFRET assays. To minimize the oligomerization of capsid 3XA or 3XC, the sample was pretreated with imaging buffer containing a different concentration of 300~1,500 mM NaCl for 30 min, and then returned to the normal level of NaCl after the protein immobilization on the slide.

The surface-bound capsid proteins were illuminated using the evanescent field generated by the total internal reflection of a 532-nm laser. Fluorescence emission was collected through a 1.49 NA 100 × oil-immersion objective (Olympus), and passed through a filter to remove Rayleigh scattering of the laser light. Acceptor and Donor emissions were separated using a dichroic mirror into green and red emissions. The two resulting emissions were projected onto the EMCCD, respectively. The single-molecule time traces of around 100 s were collected at a rate of 10 frames/second using Micro-Manager. All smFRET experiments were performed at room temperature.

Competitive Binding to Host Cells with GAGs

Soluble GAG analogs were employed as receptors. Heparin (MCE), De-N-sulfated acetylated heparin (DeN heparin; Sigma-Aldrich), bovine tracheal chondroitin sulfate A (CSA; Sigma-Aldrich) were dissolved at 2,500 μg/ml in RPMI 1640 or MEM for preincubation with VLPs or PCV2 at 37 ° C for 90 min before the mixture was added to 3D4/31 or PK15 cells for 60 min at 4 ° C to ensure effective attachment. The mixture was then washed off with phosphate-buffered saline (PBS) and the cell samples were collected and processed. The total amount of bound protein was analyzed using immunoblotting with the anti-capsid mAb 5E11 for 2 h at 37 ° C and with HRP- goat anti-mouse IgG (Kirkegaard & Perry Laboratories) for 45 min 37 ° C before chromogenic detection. The copy number of the attached PCV2 virions was determined using quantitative real-time PCR.

Flow Cytometry

The ratio of attached cells was measured using flow cytometry. Trypsin digested PK15 or 3D4/31 cells were suspended, incubated with mAb 5E11 for 1.5 h at 37 ° C, stained with FITC- goat anti-mouse IgG (Abcam) for 1 h, and evaluated using a BD Accuri™ C6 Plus flow cytometer (BD Bioscience), and the ratio was analyzed using Flow Jo X 10.0.7 software(FlowJo, LLC).

High Performance Liquid Chromatography with Heparin-Sepharose

Purified WT, SM, and DM capsid samples (100 μg) were loaded onto a 5-ml HiTrap™ Heparin-Sepharose HP Column (GE Healthcare) at a flow rate of 1 ml per minute. The column was washed with Ca^{2+} and Mg^{2+}-free PBS to remove unbound molecules, and then eluted with gradually linear increasing concentrations of NaCl. The electrostatic interactions between Heparin-Sepharose and heparin-binding proteins would be disrupted by increasing concentrations of salt. The original sample, flow through, and elution fractions of proteins were collected, diluted to same concentration, and then analyzed using SDS-PAGE and immunoblotting with the anti-capsid mAb. The intensities of the immunoreactive protein bands were measured using Image J 1.52g software.

Microscale Thermophoresis Assay

The dissociation constant values between WT, SM, and DM capsids and heparin or antibodies were measured using a microscale thermophoresis assay (MST). The Cy5-labeled protein was incubated at a constant concentration of 20 nM with two-fold serial dilutions of GAGs or antibodies in the same buffer system used for the smFRET assay. Equal volumes of binding reactions were mixed and incubated for 15 min at room temperature. The mixtures were added into glass capillaries and loaded into a Monolith NT.115 instrument (NanoTemper Technologies, Germany), and the K_d values were determined using NanoTemper Analysis software (NanoTemper Technologies).

Construction of a PCV2 Infectious Clone and Virus Rescue

Site-specific mutagenesis to construct the ^{99}R (SM) and ^{99}R^{100}K (DM) mutants was performed directly using PCR with the whole genome of PCV2 strain HZ0201. The linear genomes of the WT and mutant PCV2 were extracted, cyclized using T4 DNA ligase (Takara), and transfected into PK15 cells for virus rescue with the jetPRIME® in vitro transfection reagent (Polyplus-transfection). The transfected cells were cultured for 72 h and

continuously passaged. The rescued virus samples were evaluated using the anti-capsid mAb with an indirect immunofluorescence assay and virus titers were calculated according to the Reed-Muench method.

Analysis of smFRET Data

Using custom made IDL software (Exelis Visual Information Solutions), hundreds of FRET traces displayed anti-correlation behaviors between donor and acceptor fluorescent signal were picked from the images of an acceptor detection channel by alternating the 532 and 633 nm laser excitations, and these FRET traces were further analyzed with a Hidden Markov Model (HMM) based VBFRET software (VBFRET software package script, The Gonzalez Laboratory) by a custom-made MATLAB algorithm (Mathworks). The fluorescence traces were used to calculate the apparent FRET efficiency according to FRET = $I_A/(I_A+I_D)$, where I_A and I_D were the fluorescence emission intensities of the acceptor and donor fluorescence, respectively. The points in traces where the fluorescence intensity of donor or acceptor dropped to 0 and no longer recovered within the experimental observation time were determined as photobleaching and cut off to not be used for further analysis. The number of states in each trace was automatically set to 10 for fitting, and the states were identified according to criteria: (1) The corresponding donor and acceptor fluorescence intensity on the trace of the states displayed anti-correlation; (2) the FRET signals of the states showed a duration for minimally 10 frames. Under such criteria, three mainstream states for each trace were obtained and defined as low, intermediate, and high FRET states, and the means ± standard deviations (SD) of states FRET values of traces were defined as the state FRET efficiency levels. All the observed FRET data points until the photobleaching point were compiled into histograms using origin 9.0 software (Originlab). Overlaid on the histograms are multiple Guassian distributions. The occupancy of each Gaussian peak was calculated as the ratio of peak covering area to theaccumulated multiple Gaussian distributions, respectively. The dwell times were obtained based on states identified by HMM analysis, and compiled into histograms, fitted with a single-exponential decay curve to further extract the rate(k) of transitions between every pair of states. Results of fitting are displayed in Figure S6

Statistical Analysis.

All results are presented as means ± the SDs. Significant differences between treated and control groups were analyzed using Student's t-test. The differences were considered significant and extremely significant at P values < 0.05 and < 0.01, respectively.

Supplemental Reference

Zhou, J.Y., Chen, Q.X., Ye, J.X., Shen, H.G., Chen, T.F., and Shang, S.B. (2006). Serological investigation and genomic characterization of PCV2 isolates from different geographic regions of Zhejiang province in China. Veterinary research communications *30*, 205-220.

Zhou, Z., Cironi, P., Lin, A.J., Xu, Y., Hrvatin, S., Golan, D.E., Silver, P.A., Walsh, C.T., and Yin, J. (2007). Genetically encoded short peptide tags for orthogonal protein labeling by Sfp and AcpS phosphopantetheinyl transferases. ACS Chem Biol *2*, 337-346.

Roy, R., Hohng, S., and Ha, T. (2008). A practical guide to single-molecule FRET. Nat Methods *5*, 507-516.

Fairhead, M., and Howarth, M. (2015). Site-specific biotinylation of purified proteins using BirA. Methods Mol Biol *1266*, 171-184.

.